Shible, H., Hollender, F., Bindi, D., Traversa, P., Oth, A., Edwards, B., Klin, P., Kawase, H., Grendas, I., Castro, R. R., Theodoulidis, N., Gueguen, P. (2022): GITEC: A Generalized Inversion Technique Benchmark. - Bulletin of the Seismological Society of America, 112, 2, 850-877.

https://doi.org/10.1785/0120210242

GITEC: A Generalized Inversion Technique Benchmark

Hussein Shible*[1,2], Fabrice Hollender[1,2], Dino Bindi[3], Paola Traversa[4], Adrien Oth[5], Benjamin Edwards[6], Peter Klin[7], Hiroshi Kawase[8], Ioannis Grendas[9], Raul R. Castro[10], Nikolaos Theodoulidis[11], and Philippe Gueguen[2]

ABSTRACT

Generalized inversion techniques (GITs) have become popular for determining seismological parameters (e.g., source, attenuation, and site response), particularly in low-to-moderate seismicity regions. Indeed, GITs can potentially provide reliable site-response estimates when a minimum number of recordings is available, as well as valuable information about source parameters and regional attenuation characteristics. Significant advances have been made on GITs in which different approaches and hypotheses were investigated, such as the application of "nonparametric" and "parametric" inversion schemes. In this context, several scientific questions have arisen that depend on the final scope of the GITs: What is the optimal inversion strategy for a given dataset configuration? What is the impact of the different choices, assumptions, and implementations on the reliability of the results? Is it possible to quantify the associated epistemic uncertainties? Here, we have considered and compared the different approaches of GITs to improve the understanding of each for use in different applications. A methodological benchmark that includes different GIT methods and dataset configurations is set up to fulfill the objective, using a simple synthetic dataset, a French regional sparse dataset, and an Italian national dense dataset. The benchmark is developed in two phases: (1) phase I: a free phase with no common constraints; and (2) phase II: a constrained phase with unified reference conditions. Despite unifying the reference conditions in the different inversions, the variability was not reduced. Discrepancies are observed between different terms of GITs. Site responses appear to be the most robust estimates, compared to source and attenuation terms. The way that stress drops of earthquakes and quality factors for crustal attenuation are parameterized appears to lead to significant variability between different approaches. Finally, uncertainties are addressed by quantification of the inter-method variability for the different terms and parameters.

KEY POINTS

- The work presents a comparison of generalized inversion techniques.
- The results indicate that site terms are the most robust.
- Unaccounted complexities of ground motion in generalized inversion models can lead to increased uncertainties.

INTRODUCTION

Seismic waves initiate from seismic faults and ruptures in the Earth's crust, and propagate from the source to the Earth's surface through different paths to impact built structures and installations. The ground motions observed at the surface can be greatly affected by several factors, such as the rupture characteristics (i.e., source effects), the seismic-wave attenuation properties of the Earth materials between the source and a specific site (i.e., path propagation effects), and the amplification of ground-motion amplitudes induced by specific lithological and topographical configurations in the near-surface subsoil (i.e., site effects). After several destructive earthquakes during the last few decades (e.g., Mexico, 1985, Kobe, 1995, Haiti, 2010, and Tōhoku,

1. French Alternative Energies and Atomic Energy Commission (CEA), DES, CEA Cadarache, DCET/SESN, Saint Paul Lez Durance, France, https://orcid.org/0000-0001-8618-0150 (HS); https://orcid.org/0000-0003-1440-6389 (FH); 2. ISTerre, Université Grenoble-Alpes, CNRS, IRD, Université Gustave Eiffel, Grenoble, France, https://orcid.org/0000-0001-6362-0694 (PG); 3. GFZ German Research Centre for Geosciences, Telegrafenberg, Potsdam, Germany, https://orcid.org/0000-0002-8619-2220 (DB); 4. EDF-DIPNN-DITEGG, Aix-en-Provence, France, https://orcid.org/0000-0002-9639-7342 (PT); 5. European Center for Geodynamics and Seismology, Walferdange, Luxembourg, https://orcid.org/0000-0003-4859-6504 (AO); 6. School of Environmental Sciences, University of Liverpool, Liverpool, United Kingdom, https://orcid.org/0000-0001-5648-8015 (BE); 7. National Institute of Oceanography and Applied Geophysics (OGS), Sgonico, Trieste, Italy, https://orcid.org/0000-0002-5373-4484 (PK); 8. Disaster Prevention Research Institute, Kyoto University, Uji, Kyoto, Japan, https://orcid.org/0000-0001-8370-1707 (HK); 9. Geophysics Department, School of Geology, Aristotle University of Thessaloniki, Thessaloniki, Greece, https://orcid.org/0000-0003-4142-1795 (IG); 10. Departamento de Sismología, División Ciencias de la Tierra, Centro de Investigación Científica y de Educación Superior de Ensenada (CICESE), Ensenada, Baja California, Mexico, https://orcid.org/0000-0003-0463-0117 (RRC); 11. ITSAK, Thessaloniki, Greece

*Corresponding author: hussein.shible@seister.fr

2011), accurate evaluation of strong ground motion factors has become a necessary step for realistic prediction of the ground motion that can be expected for future strong earthquakes.

Seismic hazard assessment is carried out to predict the intensity of ground shaking either in a given region or for a specific site. In seismic hazard assessment, the ground-motion evaluation is generally carried out using ground-motion prediction equations (GMPEs), and they are determined through regression analyzes of empirically recorded data. Recently, probabilistic seismic hazard studies have been progressively refined to improve site-specific hazard estimates by relaxing the ergodic assumption (Rodriguez-Marek et al., 2013; Kotha et al., 2016). These studies require knowledge of the amplification of the ground motion at the site considered. Most of the current GMPEs base the evaluation of site responses on the V_{S30} proxy (time-averaged S-wave velocity in the first 30 m of the profile) and the high-frequency near-surface attenuation parameter, κ_0. The V_{S30} proxy can reflect some site properties, but it is not enough to describe the frequency-dependent amplification of ground motion induced by the soil properties beneath the considered site (Lee and Trifunac, 2010). In addition, several sources of uncertainties are associated with κ measurements and applications to consider local attenuation effects. As a result, there is an increased attention toward improving the practice through more precise site-effect estimations.

Within this scope, Bard et al. (2020) reviewed the main practices to obtain site-specific ground-motion predictions and provided several recommendations. One of the main recommendations was to investigate site effects with generalized inversion techniques (GITs), mainly because these represent an alternative tool for evaluating empirical site responses in the frequency domain. However, the latter use of GITs does not hide that they can deliver, along with site terms, other source, and attenuation parameters, such as stress drop and quality factors, which are of the main elements used in stochastic modeling (Boore, 2003) of earthquake ground motions. Indeed, GITs were first introduced by Andrews (1986), based on the assumption that the Fourier spectrum of a recorded seismic signal can be separated into three main components: source, path, and the site factors. Then, generalized inversions were used in numerous studies that focused on crustal attenuation (e.g., Castro et al., 1990; Parolai et al., 2004; Bindi et al., 2006), source parameters (e.g., Oth et al., 2017), and site-response estimations (Nakano et al., 2015; Edwards and Fäh, 2017; Kawase et al., 2019).

Although there are several methods for estimating source parameters, crustal path attenuation, and site responses individually, GITs are being used to estimate them simultaneously for a given dataset. The results of generalized inversions of ground motion, including source and attenuation parameters, have been used for several purposes. Bora et al. (2015) used GITs to develop a Fourier amplitude spectrum GMPE that can be adjusted to account for source, path, and site conditions for the regions of interest. The adjusting parameters were stress drops ($\Delta\sigma$), a quality factor (Q), and the high-frequency attenuation parameter κ. Perron et al. (2017) focused on the estimation of κ for sites in the Provence area of southern France, and they indirectly used GIT results of Drouet et al. (2010) to compare with the Q values obtained from the path term of κ. Based on the GIT studies of Drouet et al. (2010) in France, Drouet and Cotton (2015) also performed stochastic simulations of ground motion, and they determined fully stochastic GMPEs for southern France based on these synthetic data.

The choice of the most appropriate GIT scheme for an application might depend on the dataset geometry and characteristics. In addition, the most appropriate assumptions can vary for different dataset configurations and the aims of a study. However, these choices have not been deeply explored in the previous studies. In addition, the resulting "intermethod" uncertainty for the estimated physical parameters has not been addressed previously in the framework of detailed parameter estimation. These issues concerning intermethod variabilities were found motivating enough for us to set up an international benchmark to compare the different implementations of GITs currently in use, to investigate their advantages and drawbacks and their relative performance of each inversion technique with respect to the others, as well as to explore the uncertainty for the estimated seismological parameters from different implementations of the inversion procedure.

GITEC benchmark (Generalized Inversions

Techniques Comparisons) was organized based on the idea of performing several inversions with multiple GIT schemes on different datasets. The benchmark addresses the possible differences between different approaches on the same dataset and between different datasets. The main scope of GITEC is to compare and improve the knowledge on the performances of different generalized spectral inversion methods and the underlying hypotheses they use to estimate ground-motion parameters.

This GITEC "methodological benchmark" is expected to serve several goals:

- First, a major concern is about the optimal inversion strategy given a specific dataset. The presence of different implementations of inversion schemes (i.e., parametric, nonparametric) makes it important to investigate the pros and cons of each approach, depending on the dataset characteristics considered (e.g., dataset geometry, configuration, and others).
- Exploration of the impact of the choices, assumptions, and reference conditions on the final results.
- Addressing the quantification of epistemic uncertainties by intermethod comparisons over different datasets.

This work summarizes the results and the main conclusions reached with the GITEC benchmark. Inversions were run by the six teams that participated in the benchmark. Initially, inversions were performed on a simple synthetic dataset as a sort of "sanity check" for all inversion schemes and codes. The inversions were then performed on two real datasets available from previous studies, with some slight modifications and updates. The impact of the choice of the reference condition was explored by performing two phases of inversions (I, II), in which the reference conditions were changed from phase I to phase II. In the first run, the teams' reference conditions were freely set while unified in the second run. The impact of the dataset size on the inversion performance was also explored in two steps. First, the two datasets considered were chosen to have different numbers of records. Then, in a separate test, the number of records in one of the datasets was decimated before running the inversions.

We do not claim to present here the "best practice" for GIT applications, but instead, we aim to provide a comparison of the different existing methods to address the question of the uncertainties in GITs. In the end, analysis of the results from different approaches and inversion schemes allowed characterization of the intermethod variability. We also highlight the relative robustness of the seismological terms and the relative suitability of the different approaches as functions of the dataset configuration.

GITs

Generalized inversion schemes are based on the principle that far-field, S-wave Fourier amplitude spectra can be separated into three main components, as indicated in the following equation:

$$FAS_{ij}(f) = E_j(f)A_{ij}(r_{ij}, f)S_i(f), \qquad (1)$$

in which FAS_{ij} is the Fourier amplitude spectrum for each frequency f recorded at site i for event j, $E_j(f)$ is the source function, $A_{ij}(r_{ij}, f)$ is the path contribution over distance r for event j recorded at site i, and $S_i(f)$ is the site-response term. Each of these terms is assumed to be independent from one another for a given spectrum.

Applying a logarithm to equation (1), we obtain the linear equation that provides a linear system of the form $\boldsymbol{A} \cdot \boldsymbol{x} = \boldsymbol{b}$, in which $\cdot$ is the dot product, $\boldsymbol{b}$ is the data vector, $\boldsymbol{x}$ is the solution of the system, and $\boldsymbol{A}$ describes the system matrix (Andrews, 1986; Castro et al., 1990). In the way that this system is defined, it has two undetermined degrees of freedom. The system can then be solved if two additional constraints are applied to one (or several) site responses and to the attenuation function at a given reference distance. In GITs, this is often called the reference site condition.

An inversion scheme can be implemented following either a nonparametric or a parametric approach. The difference between these two approaches lies in the assumptions made a priori. In a nonparametric inversion, no models with predefined function are assumed a priori, and the inversion is carried out at each frequency point to separate the three contributions described in equation (1). Nonparametric inversion provides the source spectra $E(f)$ for each earthquake, the average attenuation curves $A(r, f)$ as functions of the distance at each frequency, and the site amplification $S(f)$ as a function of

frequency for all of the sites. On the other hand, analytical models are assumed to account for the source and attenuation terms in the parametric approach, whereas the site term is kept nonparametric. Parametric inversions provide the direct output of estimates of the controlling parameters for the models assumed. When performing nonparametric inversions, these parameters are instead retrieved by performing postinversion parameterization for each nonparametric term.

To run parametric inversion schemes, models must be assumed a priori. The model of Brune (1970, 1971) and Eshelby (1957) is usually used for the source term, as described in the following equations:

$$\Omega(f) = \left(\frac{2R_{\theta\phi}}{4\pi\rho\beta^3}\right)\left(\frac{(2\pi f)^2 M_0}{1+\left(\frac{f}{f_c}\right)^2}\right), \quad (2)$$

$$\Delta\sigma = \frac{7}{16} M_0 \left(\frac{f_c}{0.37 V_S}\right)^3, \quad (3)$$

in which M_0 ($N \cdot m$) is the seismic moment, f_c (Hz) is the corner frequency of the earthquake, $\Delta\sigma$ (Pa) is the stress drops, $R_{\theta\phi}$ is the source radiation pattern, which is assumed to be constant ($R_{\theta\phi} = 0.55$ for S waves; Boore and Boatwright, 1984), ρ (kg/m^3) is the average density in the crust, β (m/s) is the S-wave velocity of the medium near the source, and V_S is the average S-wave velocity along the path. In general, for earthquakes at local to regional distances, we assume that $\beta = V_S =$ 3.5 km/s and $\rho =$ 2800 kg/m^3, as in several studies (e.g., Drouet et al., 2010; Bindi et al., 2017). With M_0 obtained from inversions, the moment magnitude M_w can be deduced using the relation of Hanks and Kanamori (1979), as in the following equation:

$$M_w = \frac{\log_{10}(M_0) - 9.05}{1.5}. \quad (4)$$

The attenuation of seismic waves is acquired by waves propagating through the crust, so it is usually constrained to unity at the nearest possible to the source. In the nonparametric approach, the attenuation is derived directly over the available distance bins in the data. When we have no data at short distances, the attenuation is fixed to 1 at a distance defined as the reference distance (R_{ref}). This assumption leads to shifted sources at the chosen R_{ref}. Thus, nonparametric source terms need to be rescaled by R_{re} for correct interpretation. The path term assumed accounts for both anelastic attenuation and the geometrical spreading decay effects, as given by the following equation:

$$A(r,f) = \exp\left(-\frac{\pi(r - R_{ref})f}{Q_0 f^{\alpha} V_S}\right)\left(\frac{R_{ref}}{r}\right)^{\gamma}, \quad (5)$$

in which Q_0 and the exponent α describe the frequency-dependent quality factor, and γ is the coefficient of the geometrical spreading. It is worth noting that in a parametric approach, R_{ref} is implicitly set to 1.

Here, an additional attenuation representation is proposed for the quality factor, Q. A more generalized evaluation of Q, which is mainly assumed as $Q_0 f^{\alpha}$ in equation (5), can be provided for a given distance and frequency. We chose to evaluate the generalized Q at 50 km, in which attenuation is not yet undergoing additional complexities, and in which we can consider that $\gamma = 1$. Also, we chose the frequency to be in the middle of the frequency range considered in the dataset. Indeed, other choices are also possible for detailed interpretations, but we considered only one (r, f) couple, with the general notation $Q_r(f)$. The main consequences of such a parameterization are:

- Having an alternative to the actual Q-model parameters can show better how much the approaches are consistent in their attenuation.
- That the $Q_r(f)$ term reveals more information attenuation than the Q_0 value.

The $Q_r(f)$ term can be improved for better interpretation of the attenuation properties. However, it appears a good start to exclude possible trade-offs (i.e., among Q_0, α, and γ) from the comparisons.

THE GITEC PROJECT

Methodologies and inversion schemes involved in the benchmark

The GITEC benchmark includes several inversion schemes, as listed in Table 1, and these can be classified into three main categories:

- Full nonparametric inversion schemes. These inversions can be carried out as:
  1. One-step inversion, including simulta-

TABLE 1
Inversion Schemes of the GITEC Benchmark

No.	Inversion Method	Team	Affiliation	Scheme	Code
1	Oth et al. (2011)	Adrien Oth, Dino Bindi	ECGS, Luxembourg; GFZ Potsdam, Germany	Nonparametric (one-step inversion)	#01N1
2	Klin et al. (2018)	Peter Klin	OGS, Trieste, Italy	Nonparametric (two-step inversion)	#02N1
3	Castro et al. (1990)	Raul Castro	CICESE, Mexico	Nonparametric (two-step inversion)	#03N2
4	Drouet et al. (2010)	Hussein Shible	CEA-Cadarache, France	Parametric	#04P
5	Nakano et al. (2015)	Hiroshi Kawase	Kyoto University, Japan	Semiparametric	#05SP
6	Grendas et al. (2021)	Ioannis Grendas Nikolaos Theodoulidis	AUTh, ITSAK, Greece	Parametric	#06P
7	Edwards et al. (2008)	Ben Edwards	University of Liverpool, United Kingdom	Parametric	#07P

AUTh, Aristotle University of Thessaloniki; CEA, French Alternative Energies and Atomic Energy Commission; CICESE, Centro de Investigación Científica y de Educación Superior de Ensenada; ECGS, European Center for Geodynamics and Seismology; ITSAK, Institute of Engineering Seismology and Earthquake Engineering; OGS, National Institute of Oceanography and Applied Geophysics.

neous inversion of each of source, path attenuation, and site-response terms in equation (1). In this approach, a single matrix of the system of unknowns is first formed, and then it is solved. The used methods were:
    - The scheme developed by Bindi et al. (2009) and Oth et al. (2011) was run. In the following, these inversions have the reference #01N1.
    - The scheme developed by Klin et al. (2021) which is an improvement of the scheme of Klin et al. (2018). In the following, these inversions have the reference #02N1.
  2. Two-step inversion, in which the attenuation is first solved in single step, then the source and site are afterward solved by correcting the Fourier spectra for the attenuation obtained from the first step. The two-step nonparametric inversion scheme run was the scheme developed by Castro et al. (1990). In the following, these inversions have the reference #03N2.
- Full parametric inversion schemes, divided into the following different inversion schemes:
  1. The scheme implemented by Drouet et al. (2010). In the following, these inversions have the reference #04P.
  2. The same scheme implemented by Drouet et al. (2010), but further redeveloped, modified, and optimized by Grendas et al. (2021), using a single attenuation model. In the following, these inversions have the reference #06P.
  3. The scheme implemented by Edwards et al. (2008). In the following, these inversions have the reference #07P.
- Semiparametric (or partially nonparametric) inversion schemes, in which only the attenuation model is parameterized with a Q model and a geometrical spreading factor, whereas the source and site terms are kept nonparametric. This scheme was implemented by Nakano et al. (2015). In the following, these inversions have the reference #05SP.

The datasets considered

To investigate the performances of the different GIT schemes with respect to different datasets, we considered:

- A synthetic dataset (as detailed in Goertz-Allmann and Edwards, 2014) generated as a forward problem solution according to equation (1) (Fig. 1a–c). The "as recorded" noise at the corresponding station and event time is added to the synthetic signals to provide realistic spectra with bandwidth according to the event size, distance to station, and general noise level. Alternate parameter setups (e.g., attenuation, stress drop, etc.) can be utilized. The dataset configuration is based on the geometry of the existing Swiss national seismic network (as of Goertz-Allmann and Edwards, 2014), with events in the magnitude range of 3.0–5.5. The generated signals are from 50 stations and 100 events. Hypocentral distances are in the range of 0–200 km.
- A sparse regional dataset as the RAP dataset (RAP: French Permanent Accelerometric Network) in the French Alps region from Drouet et al. (2008, 2010). The final dataset (Fig.

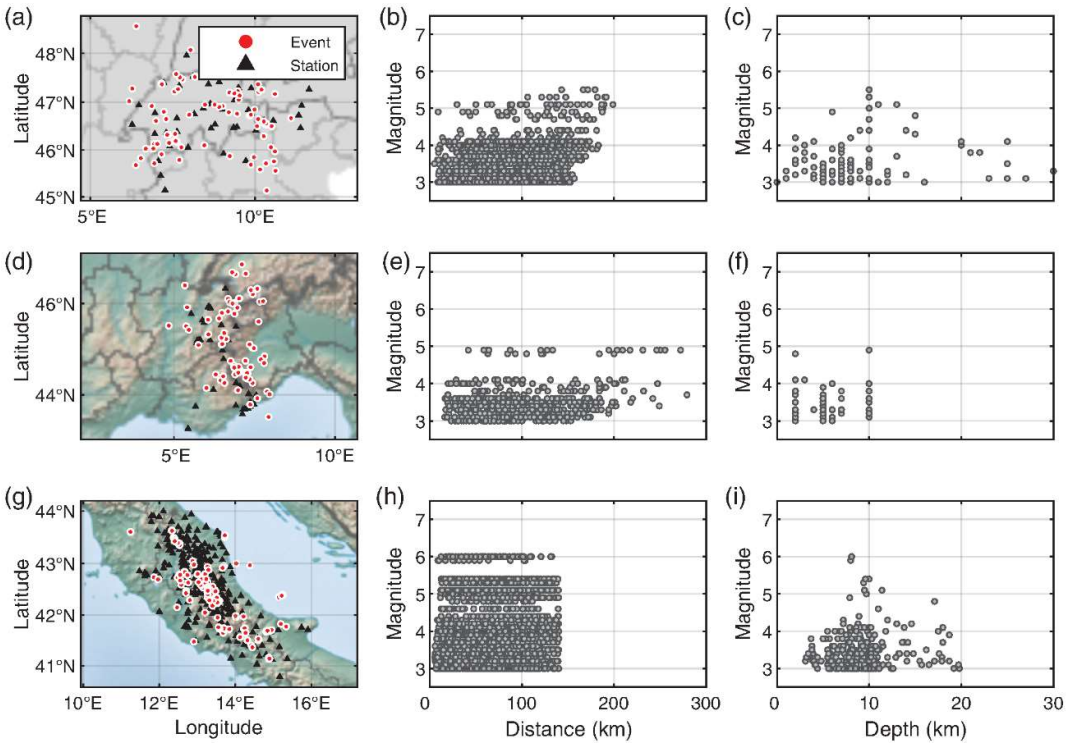

Figure 1. *(a,d,g) Maps showing the synthetic dataset and the earthquakes and stations for France and central Italy. (b,e,h) Magnitudes and hypocentral distances for the respective datasets. (c,f,i) Depth distribution of the respective sets of events, with magnitudes. Local magnitudes M_L were considered for the French and Italian data.*

1d,e) consists of 72 earthquakes in the Alps area (recorded between 1998 and 2006) with hypocentral distances of up to 250 km. The hypocentral distances of the recorded events come from the French national network agency (RéNaSS), and the local magnitudes from RéNaSS and LDG (LDG: the Geophysical and Detection Laboratory of the French Alternative Energies and Atomic Energy Commission). Focal depths range between a few kilometers and 10 km. We also note that there are other updated databases (e.g., Traversa et al., 2020) that were not considered, with the aim to test the GIT performance on data-poor and less-constrained datasets.

- A very dense regional dataset from central Italy. Data are from Bindi et al. (2017) and Pacor et al. (2016), with some updates and extensions. The dataset considered (Fig. 1g–i) consists of 231 earthquakes that were recorded by 309 stations, which include the 2009 L'Aquila sequence (mainshock M_w 6.1), and spans the period from July 2008 to January 2017. In this dataset, the local magnitudes vary in the range from 3.0 to 6.1 and are mainly concentrated within the 3.0–4.5 range. The hypocentral distances are up to 140 km, and the depths of earthquakes are mainly between 5 and 10 km.

Addressing the main objectives of GITEC requires performing consistent and reliable comparisons of results provided by the different approaches and schemes. So, it was essential to provide synthetic datasets that serve as a control for inversion results and the associated variability. The advantage of using a synthetic dataset is that the inversion is performed over data obtained directly from the forward problem, so the underlying seismological parameters are known a priori. Absolute differences between true and inverted parameters can therefore be assessed. However, the inversion of synthetic data also presents the "best-case" scenario, which may therefore underestimate methodological epistemic uncertainty. It is therefore important to also include real data and assess the relative differences between results, in spite of not knowing in which the true results lie.

The two phases and the reference conditions

First, generalized inversions on the real datasets were carried out without any a priori common constraints or assumptions; that is, each team performed the inversions independently. This starting phase (phase I) was important in

TABLE 2
Reference Sites Considered in the French and Italian datasets for Phase I, the Free Phase

Dataset	Inversion	R_{ref} (km)	Reference Site
France	#01N1	20	OGLE, ISOL
	#02N1	16	CALF, ISOL, NBOR, OGAN, OGCH, OGFB, OGGM, OGLE, OGMU, SAOF, STET
	#03N2	1	BELV, CALF, NBOR, OGAG, OGAN, OGCH, OGDI, OGGM, OGMO, OGMU, OGSI, OGTB, SAOF
	#04P	1	CALF, ISOL, NBOR, OGAN, OGCH, OGFB, OGGM, OGLE, OGMU, SAOF, STET
	#06P	1	CALF, ESCA, ISOL, MENA, NBOR, OGAG, OGAN, OGCA, OGCH, OGDI, OGGM, OGLE, OGMA, OGMB, OGMO, OGMU, OGSI, OGTI, SAOF, STET
	#07P	1	None
Central Italy	#01N1	20	MNS, RM06, RM08
	#02N1	20	CLN, LSS
	#04P	1	CLN, LSS
	#05SP	1	CLN, LSS
	#06P	1	All sites with "rock" classification following EC8 classes provided with the dataset, based on V_{S30} inferred or measured values.
	#07P	1	None

exploring the different choices to solve the inverse problem and eventually exploring the resulting variability. Indeed, constraints can vary depending on the scheme followed. However, the common constraint types between the exploited approaches were mainly the choice of R_{ref} and the reference site condition.

The reference distances and the sites for attenuation and amplification were chosen independently in phase I, as reported in Table 2. For R_{ref}, its definition was essential in the nonparametric approach, whereas it was indirectly set to 1 in the parametric and semiparametric approaches. The reference site choices were based either on trial inversions to identify flat responses or previous studies from the literature that used similar datasets. The aim behind phase I was to quantify the global epistemic uncertainty resulting due to different choices and inversion implementations.

In phase II of the inversions on the same real datasets, reference conditions were unified as much as possible. R_{ref} was set to 20 and 10 km in the nonparametric inversions for each of the French and Italian datasets, respectively. The correct choice of reference site generally requires a priori knowledge about the site conditions. Therefore, the inversions were constrained by selecting reference sites from those that were well characterized (i.e., with measured velocity profiles available).

First, the selected sites were associated with rock geological conditions, that is, V_{S30} > 1000 m/s, with at least 20 records. For the French stations, the V_{S30} was obtained from the characterization campaign data of Hollender et al. (2018). Then, one-dimensional SH-wave (1DSH) numerical simulations were carried out to estimate the theoretical elastic transfer functions using the V_S profiles provided. The 1D reflectivity model (Kennett, 1974) was used to derive the responses of the horizontally stratified layers excited by a vertically incident SH-plane wave (original software written by Gariel and Bard, and used previously in a large number of investigations, e.g., Bard and Gariel, 1986; Cadet et al., 2012; Laurendeau et al., 2018). We aimed to select the stations with the flattest site responses from the 1DSH simulations as the reference sites in the inversions. This procedure led to the choice of stations OGCH and LSS as the reference stations for the French and Italian datasets, respectively. The theoretical site responses that were fixed in the inversions are shown in Figure 2.

Intermethod comparisons were only undertaken in phase II, in which all teams used the same reference condition. In this section, detailed analyses are conducted before the evaluation of the intermethod variability. Individual source-by-source or site-by-site comparisons are avoided in this text. Only the global statistical analyses are addressed here for simplicity and clarity.

RESULTS

Inversions using the synthetic dataset

Performing an initial sanity check with a

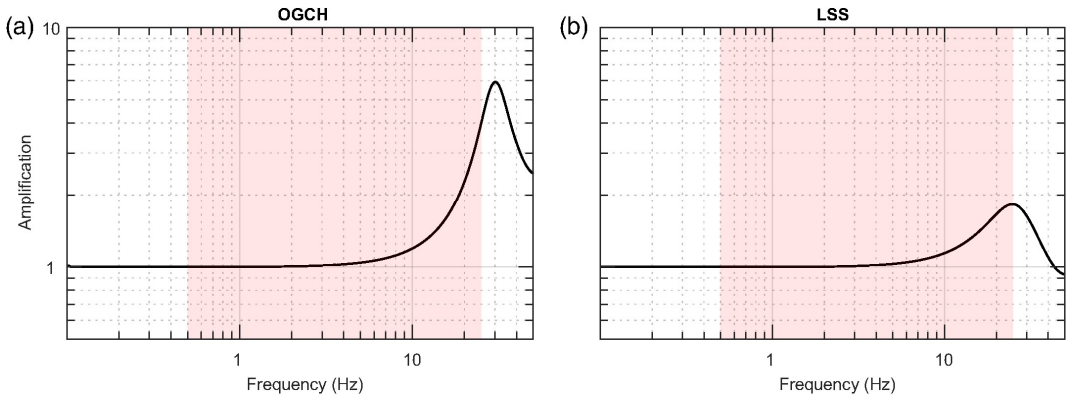

Figure 2. *Amplification functions for each of the chosen reference stations (a) OGCH and (b) LSS, as estimated from the One-dimensional SH-wave (1DSH) numerical simulation based on the available V_S profiles. The bandwidth used is shaded in red.*

synthetic dataset using a simple model parameterization helped to avoid ambiguities in the results that might make the interpretations difficult. It also provides a baseline upon which model-to-model variability can be based. Synthetic data were generated using the 50-bar Brune model for the sources, with a homogenous attenuation model for the earth crust with a quality factor $Q = 600$ (frequency independent). The reference (nonamplifying) site was also provided as input to the teams.

The results provided by the different inversion schemes led to broadly the correct parameter values, as highlighted by the $M_{w,GIT}$-M_L plots in Figure 3. Comparing the inverted corner frequencies within the range [0.3–10 Hz] with the inverted M_w showed that the stress drops obtained varied within the range of 35–60 bars, which is considered acceptable knowing that the correct values of the stress drops used in the generation of the synthetic dataset were 50 bars.

The attenuation values obtained by the different teams are considered acceptable compared with the values used in the synthetics (Table 3). Among the remaining methods, in general, all models slightly overestimate the frequency dependence of Q (as defined by α in $Q(f) = Q_0 f^{\alpha}$) and underestimate the reference Q_0. The geometric spreading rates were universally well recovered. This difference gave a first indication that we might face strong trade-offs when dealing with attenuation parameters. On the other hand, the inverted site terms were consistent with the true site amplification. Finally, this test on such a simple dataset appeared beneficial and allowed some code adjustments that were helpful in the continuation of the exercise.

Results for the sparse regional dataset, using the French Alps dataset

Comparisons of the results from the different inversion schemes are provided here for the French dataset. As shown in Figure 4, the variability in the attenuation appeared low when limiting the comparison within each type of approach (i.e., nonparametric, parametric). However, more significant discrepancies were observed in the attenuation curves at large

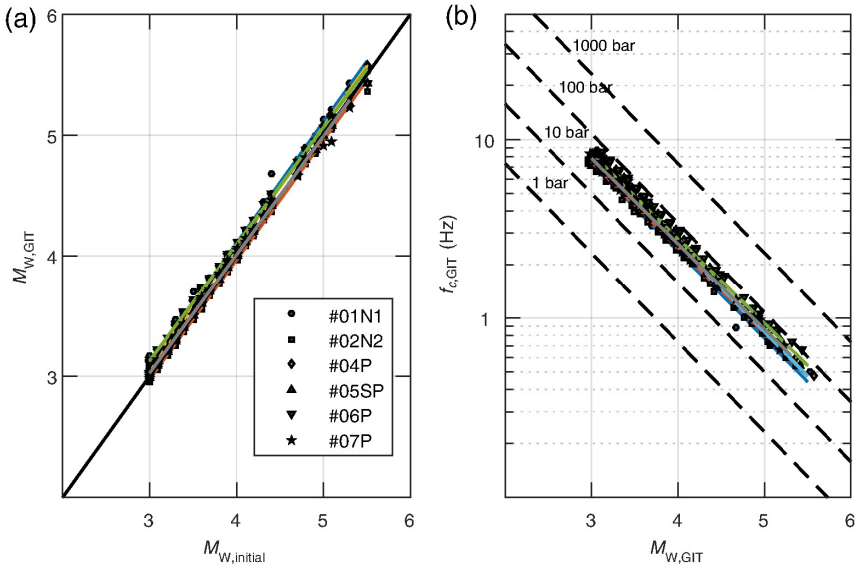

Figure 3. *Synthetic dataset for source results. (a) The 1:1 plot of the Mw obtained from the inversions ($M_{w,GIT}$) with respect to the input magnitudes (M_L). (b) Corner frequencies versus inverted M_w showing the stress-drop distributions that resulted from the inversions. Dashed lines show increasing (from bottom to top) stress-drop levels of 1, 10, 100, and 1000 bars.*

TABLE 3
Mean Estimations of the Attenuation Parameters from the Different Inversions for the Synthetics Dataset

Inversion	Q_0	α	γ
Synthetic	600,00	0,00	1,00
#01N1	533,00	0,06	1,02
#02N1	517,64	0,07	0,99
#04P	555,87	0,03	0,99
#05SP	539,08	0,04	1,00
#06P	504,62	0,06	0,97
#07P	514,00	0,05	0,98

distances, even when comparing within each type of approach. The wide range of distances in the dataset probably increased the complexity for the attenuation model for distances >100 km. These complexities might be better captured with nonparametric attenuation functions that are derived directly from the data. For example, between 50 and 200 km, the low-frequency attenuation showed discrepancies up to a factor of 4 between the parametric and nonparametric approaches. At high frequencies, these discrepancies can increase to a factor of around 10 for large distance ranges.

Table 4 summarizes the attenuation parameters that were obtained by the inversion schemes. The parameters provided by the different participating teams show significant variability for both of the inversion phases: the quality factor Q_0 from 55 to 390; the frequency dependence α from 0.3 to 1.1; and the geometrical spreading γ from 0.7 to 1.3. For some of the inversions, the attenuation was not affected by the reference choices, as for #03N2 and #07P mainly, as the reference choice does not affect the attenuation terms in these inversions. For some of the results that were very similar for the nonparametric attenuation (e.g., #01N1, #02N1 in phase I), the Q_0 values were different, which highlights the strong trade-off between the parameters (Q_0, α, and γ). The other representation of Q (i.e., $Q_r(f)$ was estimated at 50 km and 4 Hz; $Q_{50\text{ km}}4$ Hz)) resulted in values that were more consistent within each approach type (i.e., either parametric or nonparametric). The $Q_{50\text{ km}}(4\text{ Hz})$ representation reflects more what is observed with the nonparametric attenuation curves in Figure 4. Furthermore, these estimations were not greatly affected between the two phases of the inversions.

Figure 5 shows the source term results from the two phases of the inversions. Acceleration source spectra are compared between the nonparametric approaches with the fitted Brune model from the parametric inversions. The discrepancies reach a factor of 10 for the mean source spectra (for all of the events) obtained from each inversion scheme. In addition, variable slopes are clearly seen between the inversions at high frequencies, with variation across negative and positive values.

Figure 6 shows the mean site responses from the different inversions of phases I and II. Differences can be clearly seen for both the phases, with a factor of around 3 at the lower frequencies that increases to 10 times or higher at high frequencies. Thus, unifying the reference conditions provides more comparable mean amplifications (especially for the nonparametric approach) at lower frequencies, but there was no decrease in the variability at higher frequencies.

If we compare both sources and sites, it can be seen that the approach that results in the higher high-frequency slope on the sources corresponds to the lower slope on the site terms. After conducting phase I only, these slope observations were attributed to different choices of the reference site in phase I, which was one of the main motivations for carrying out phase II of the

TABLE 4
Summary of the Mean Estimations of the Attenuation Parameters for French Dataset from the Different Inversions for Phases I and II

	Q_0		$Q_{50\text{ km}}(4\text{ Hz})$		α		γ	
Inversion	Phase I	Phase II	Phase I	Phase II	Phase I	Phase II	Phase I	Phase II
#01N1	277.64	80.82	38.73	38.55	0.51	1.02	1.26	0.76
#02N1	55.28	68.73	40.16	41.92	1.12	1.12	0.58	0.87
#03N2	76.75	75.75	45.97	45.97	1.03	1.03	0.70	0.70
#04P	239.68	341.73	118.68	118.68	0.44	0.31	1.08	1.07
#06P	236.68	389.33	121.43	121.43	0.45	0.27	1.01	1.07
#07P	203.00	203.00	151.32	151.32	0.52	0.52	0.97	0.97

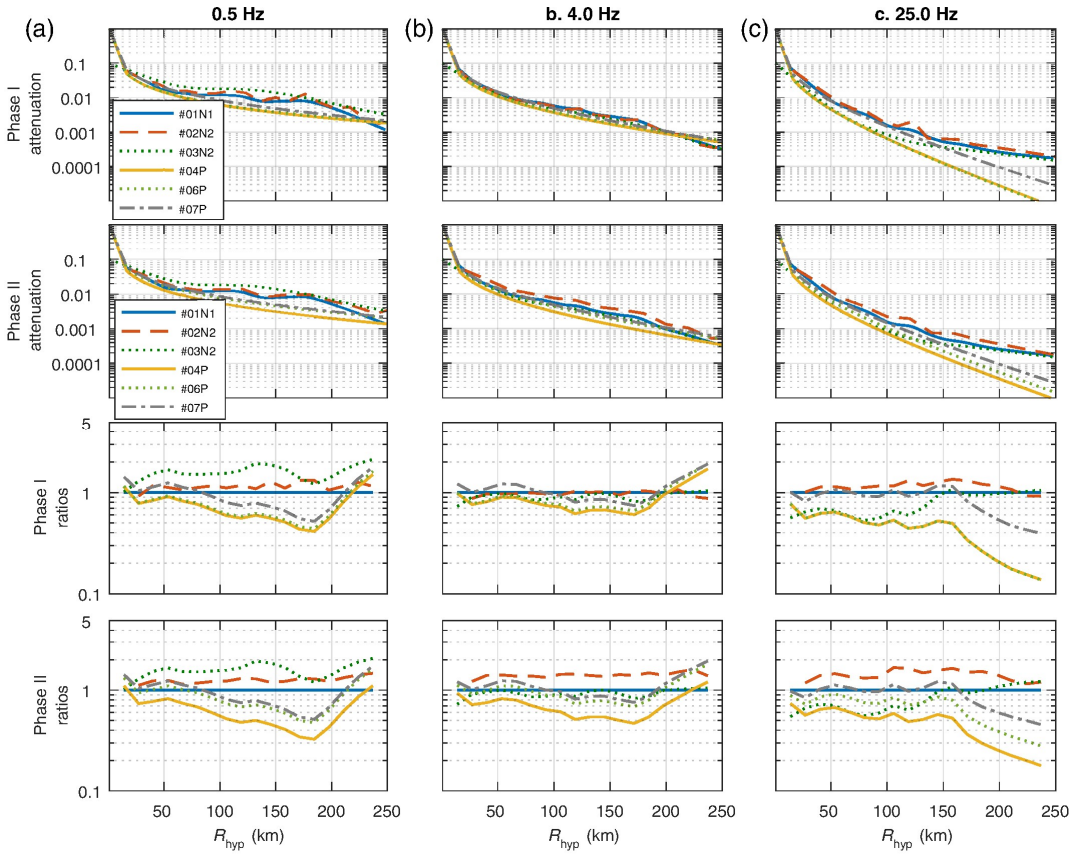

Figure 4. *French dataset results from phases I and II. (Top) Attenuation curves from the different approaches for the three frequencies, (a) 0.5, (b) 4, and (c) 25 Hz, plotted as functions of the hypocentral distance. (Bottom) Ratios of the attenuation curves with respect to #01N1.*

iterations. However, the high-frequency variability remained significant and was not reduced in phase II. Nevertheless, these data show that there is generally an impact of the choice of the reference condition on the source spectra obtained, so this choice represents an important step in the inversions.

Next, we explored the impact of these differences resulting from inversion in terms of nonparametric curves on estimating the physical parameters. A postinversion parameterization was performed to estimate M_w, f_c, and $\Delta\sigma$. To conduct consistent comparisons with the parametric inversions, the same models assumed in these schemes were used to postfit the nonparametric source spectra (equation 2). Figure 7a shows the M_w obtained from the inversions versus the M_L of the original dataset. Limited dispersion can be seen among the results for both the phases I and II, which is not the case for the other source parameters.

Figure 7b,c shows the $f_{c,GIT}$–$M_{w,GIT}$ and $\Delta\sigma_{GIT}$–$M_{w,GIT}$ distributions, respectively. Significant discrepancies can be seen for the mean $\Delta\sigma$ between the phases I and II. This reflects important variability, despite the unifying of the reference sites in phase II. The estimated $\Delta\sigma$ provided by approaches #01N1, #02N1, and #06P lie in the range of 0.1–10 bars, whereas the approaches #04P and #07P result in $\Delta\sigma$ values in the range of 1–1000 bars, with means of around 10 and 100 bars, respectively. These data highlight that the intermethod variability for these source parameters is significant even when the reference site conditions are fixed (i.e., in phase II).

Results for a dense regional dataset, using the central Italian dataset

Following the French dataset inversions, the results from the Italian dataset are presented in this section. At first glance, the path terms appear to show good agreement between the different approaches. However, when the ratios were computed with respect to one of the specific teams (#01N1), the intermethod differences reached a factor of 4, which was relatively large (Fig. 8). In phase I, the nonparametric approaches appeared to have close estimations at all frequencies and distances (#01N1, #02N1),

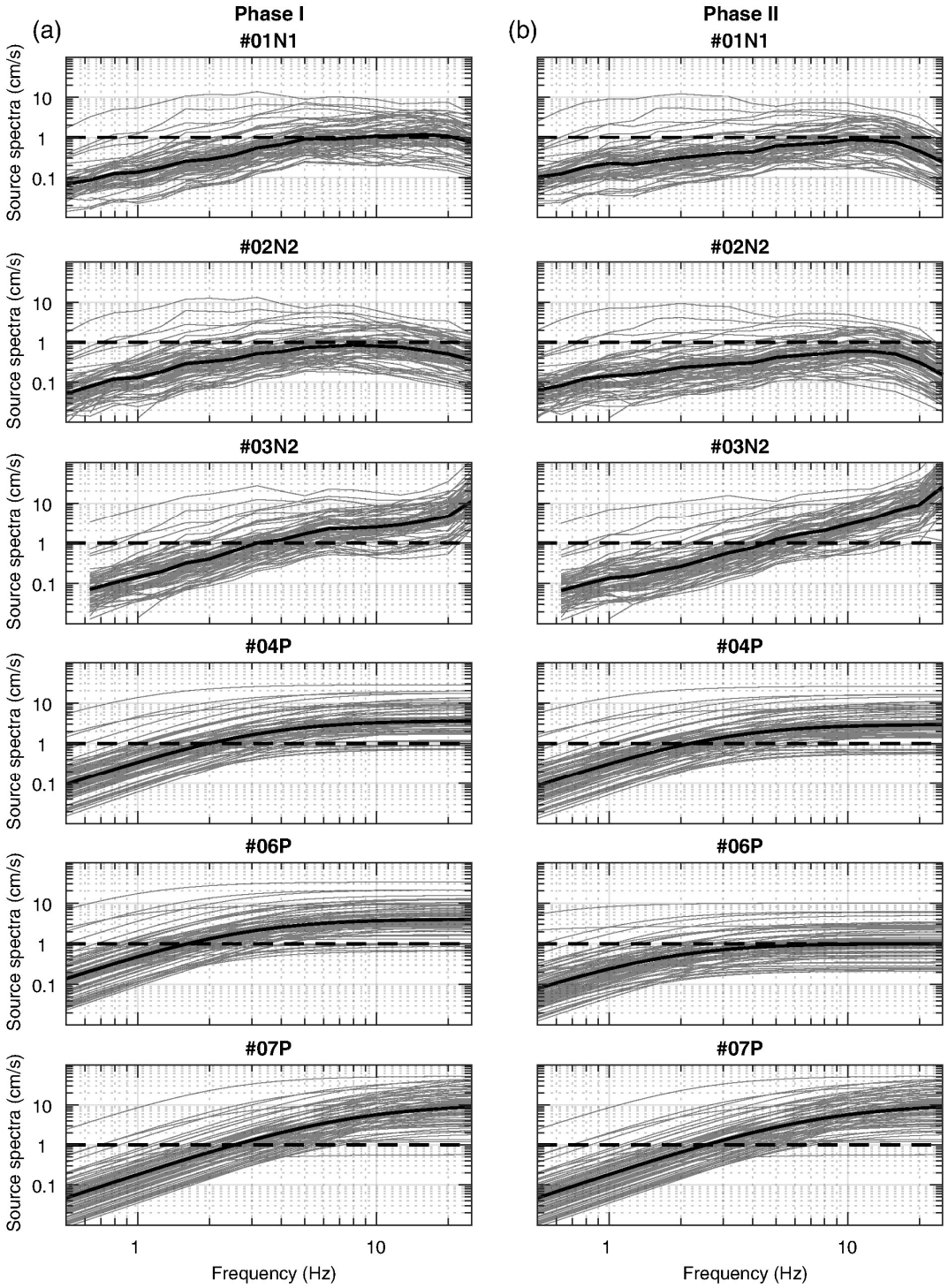

Figure 5. *French dataset results from phases (a) I and (b) II. Overall comparisons of the source spectra obtained from the different inversions (as indicated) and showing the means for all of the spectra (bold black).*

whereas the parametric approaches showed relatively variable curves. In phase II, the attenuation curves from all of the approaches were variable despite the unified reference station. Thus, significant variability affects these attenuation terms, even though the distance range was limited to 140 km.

The data presented in Figure 9 show the source spectra obtained from the different schemes. For phase I, the data showed comparable shapes of the source spectra, with small differences in amplitude at high frequencies. However, for phase II, the high-frequency slopes of source spectra appeared variable, with a tendency to decay beyond 10 Hz for the nonparametric approach of source spectra. Within each

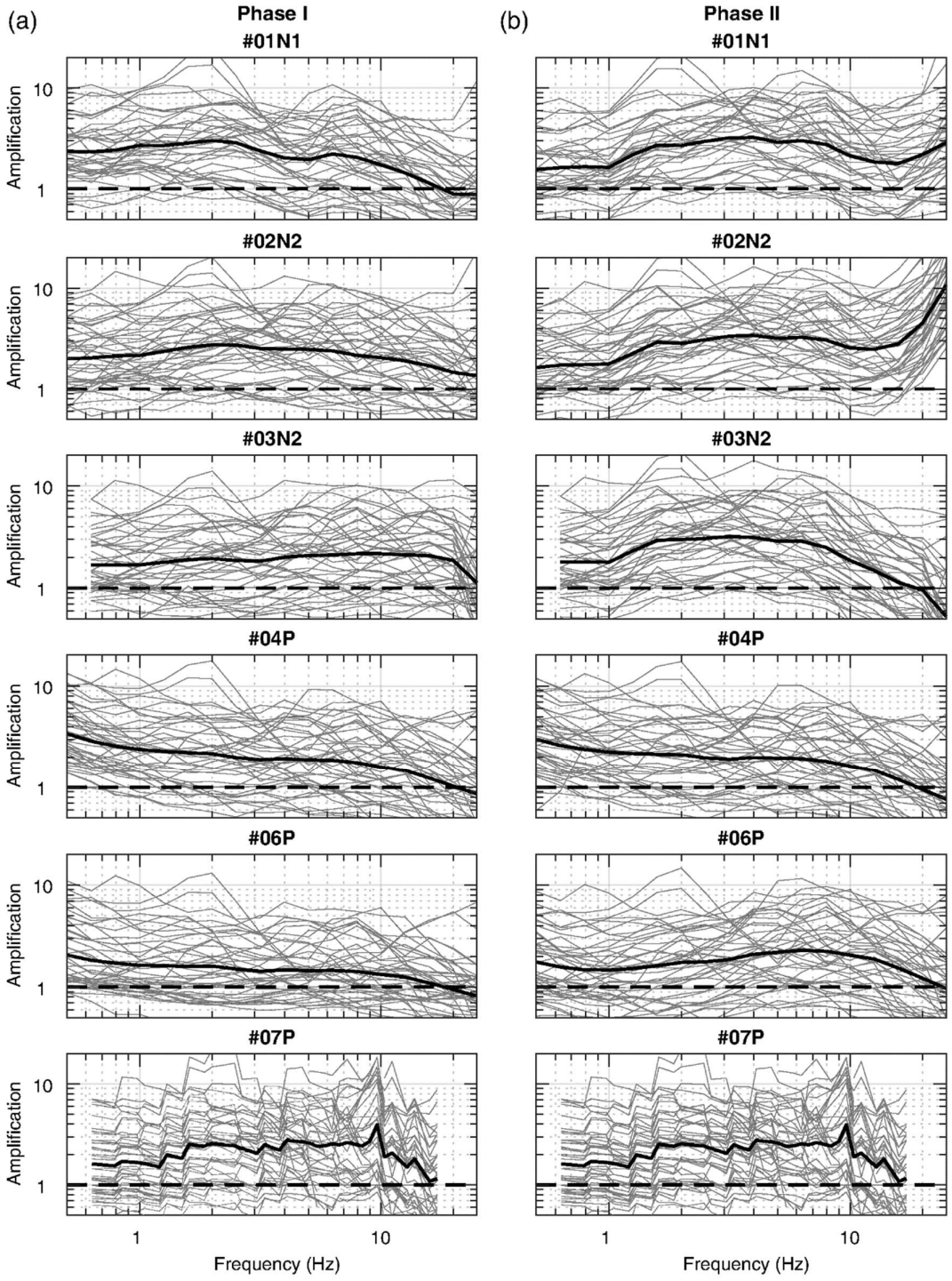

Figure 6. *French dataset results from phases (a) I and (b) II. Overall comparisons of the site amplifications obtained from the different inversions (as indicated) and showing the means for all of the sites (bold black).*

type of inversion, consistent results were obtained. With the parametric source spectra being fixed to the Brune model, the high-frequency decay of the source terms is not possible (i.e., #07P, #04P, #06P inversion schemes).

Table 5 shows the results for the attenuation parameterizations, in which greater variability is seen for the Q_0 values as well as for α and γ. For instance, the Q_0 values range from 45 to 500, along with variations in α and γ, which shows the significant trade-offs among these parameters. This might be due to trade-offs induced by the simplicity of the attenuation model used, which excludes any possible slope changes with distance (i.e., geometrical spreading effects) or by neglecting the possible regional variations. For the $Q_{50\,\mathrm{km}}(4\ \mathrm{Hz})$ representation, the values are more consistent (between different inversions)

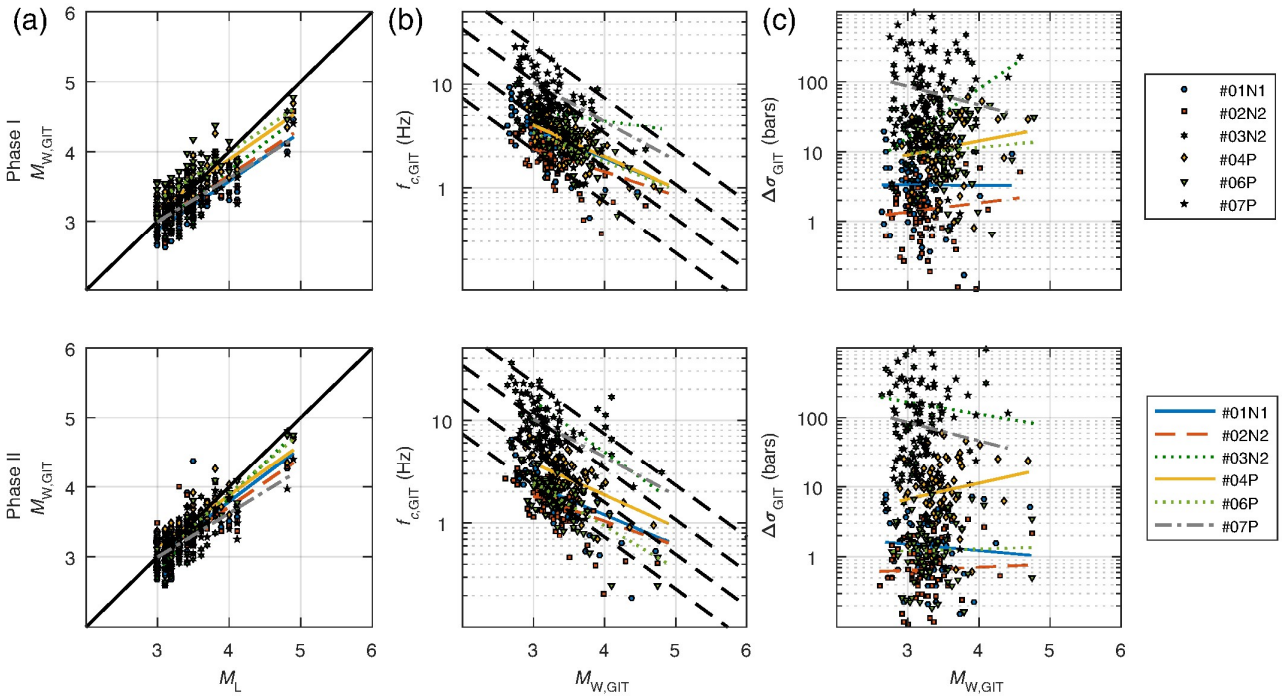

Figure 7. *French dataset source results. (a) Plot (1:1) of the M_w from the inversions ($M_{w,GIT}$) with respect to M_L values provided. (b) Distribution of the corner frequencies f_c versus $M_{w,GIT}$ estimated from the inversions. Dashed lines, stress-drop lines of 1, 10, 100, and 1000 bars. (c) Stress-drop distributions from the generalized inversion technique (GIT) approaches versus the $M_{w,GIT}$. The linear trend is shown in each plot for each inversion (with color and dashing codes in the legends).*

than seen for the Q_0 values, with also little changes between phases I and II. Although the variability is reduced with the $Q_{50\,km}(4\,Hz)$ representation, it is still present and reflects the discrepancies observed in Figure 8.

Figure 10 shows the overall views of the site term estimations provided by the different teams. The main observations for the Italian site amplifications are the differences in the high frequencies. Phases I and II show that the inversions can give different responses to the same reference site at high frequencies. For example, both methods showed changes of the slope, as for #01N1 and #02N1, whereas other inversions, such as #04P, #06P, and #07P, were not greatly affected. This appears to be partially counterbalanced by the larger high-frequency decay in the source spectra obtained by these inversion schemes, highlighting the evident trade-off between these two terms.

Although the semiparametric approach (#05SP) was applied in phase II only, it showed a decay on the source spectra. This suggests that high-frequency decay of the source spectra cannot be avoided by estimation of the attenuation parameters first in a two-step inversion to avoid the source–site trade-offs.

Comparisons of source parameters obtained directly from the parametric inversions or postinversion fitting of the nonparametric schemes are shown in Figure 11. The M_w–M_L plots show some consistency, in which the GIT results show higher values to low M_L and lower values to high M_L. This consistency was maintained between phases I and II. The stress drops $\Delta\sigma$ again showed significant variability in both the phases I and II, along with the corner frequencies, $f_{c,GIT}$. In general, the parametric schemes resulted in higher $\Delta\sigma$ than the nonparametric schemes, although within-type variability was also significant.

UNCERTAINTIES ASSOCIATED WITH THE GIT RESULTS

One of the main objectives of the GITEC benchmark was not only to investigate but also to quantify the overall uncertainties associated with the GIT data. Generally speaking, uncertainties can result from either uncertainty in the estimates of the seismological parameters provided by a given inversion scheme (i.e., intramethod uncertainties) or epistemic uncertainties related to the choice of the inversion scheme (i.e., intermethod uncertainties) and to the characteristics of the dataset on which the GIT is based. The intramethod uncertainties can

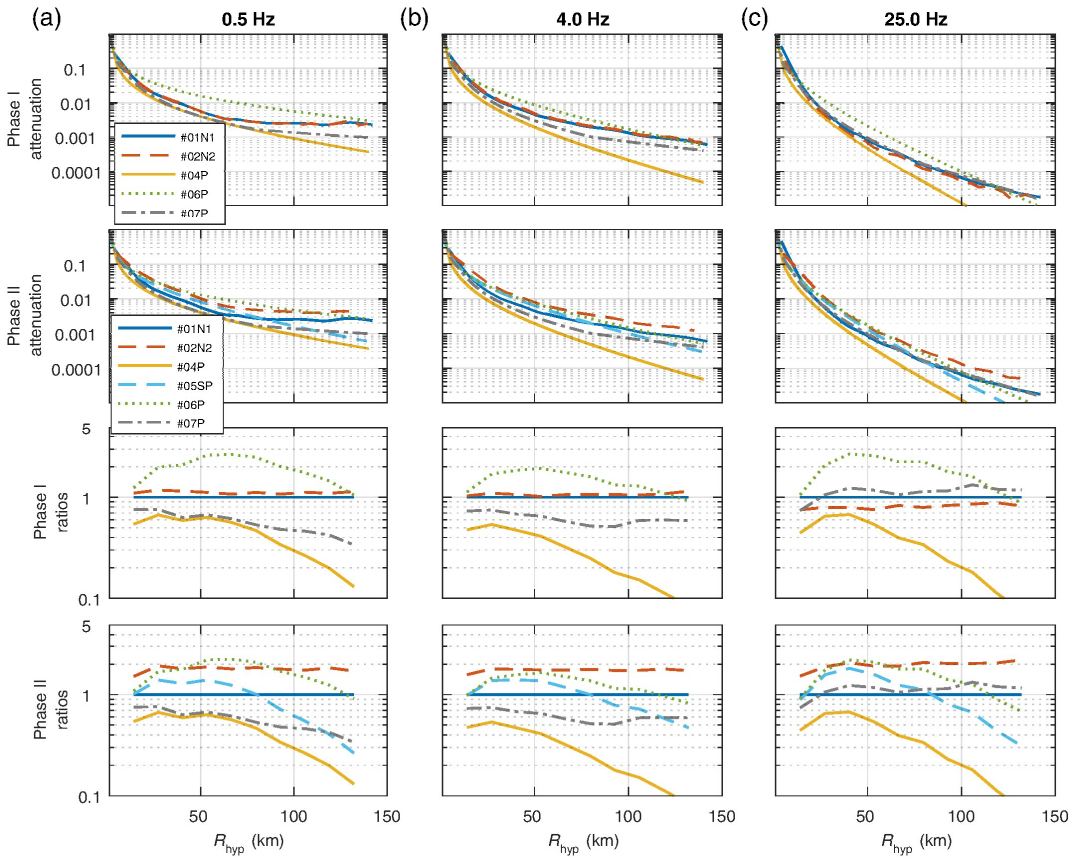

Figure 8. *Central Italian dataset results from phases I and II. (Top) Attenuation curves from the different approaches for the three frequencies, (a) 0.5, (b) 4, and (c) 25 Hz, plotted as functions of the hypocentral distance. (Bottom) Ratios of the attenuation curves with respect to #01N1.*

be described by the standard deviations associated with the results of the selected inversion procedure. The intermethod uncertainties can be captured by exploring the variability of the results provided by the different inversion approaches for the different dataset configurations. Here, we explored the intermethod variability, focusing only on phase II of the iterations for simplicity. Finally, a representative short summary of results is provided for both the phases.

Strategy for characterization of intermethod uncertainties

Given that the parametric and nonparametric inversion approaches do not provide the same results as the direct output (i.e., parametric inversions provide direct estimates of the seismological parameters, whereas nonparametric inversions provide spectral curves of the source, attenuation, and site terms), the comparisons of the variability of the results are best carried out in two steps.

The intermethod uncertainties were first quantified for the nonparametric spectra of the source, attenuation, and site terms. Because the parametric GIT provides only parameters, the source spectra and attenuation curves were reconstructed from their models. The second step was to quantify the variability for the estimations of the physical parameters. For the nonparametric approaches, postinversion parameterizations were considered (using the hypotheses and models consistent with those adopted by the parametric inversion schemes and previously presented in the text). In the end, the full (i.e., parametric and nonparametric) intermethod variability can be analyzed for each dataset considered. To determine a sort of minimum level variability, the quantification was performed over the synthetic dataset. Then the variabilities associated with the real dataset inversions are presented.

It is generally known that when uncertainties are addressed, large numbers of observations or estimations are needed to obtain meaningful statistics. However, for this benchmark, only a total of six inversion schemes were applied to each dataset. On this basis, other forms of variability indicators are defined and adopted. First, the standard deviations are calculated in the natural

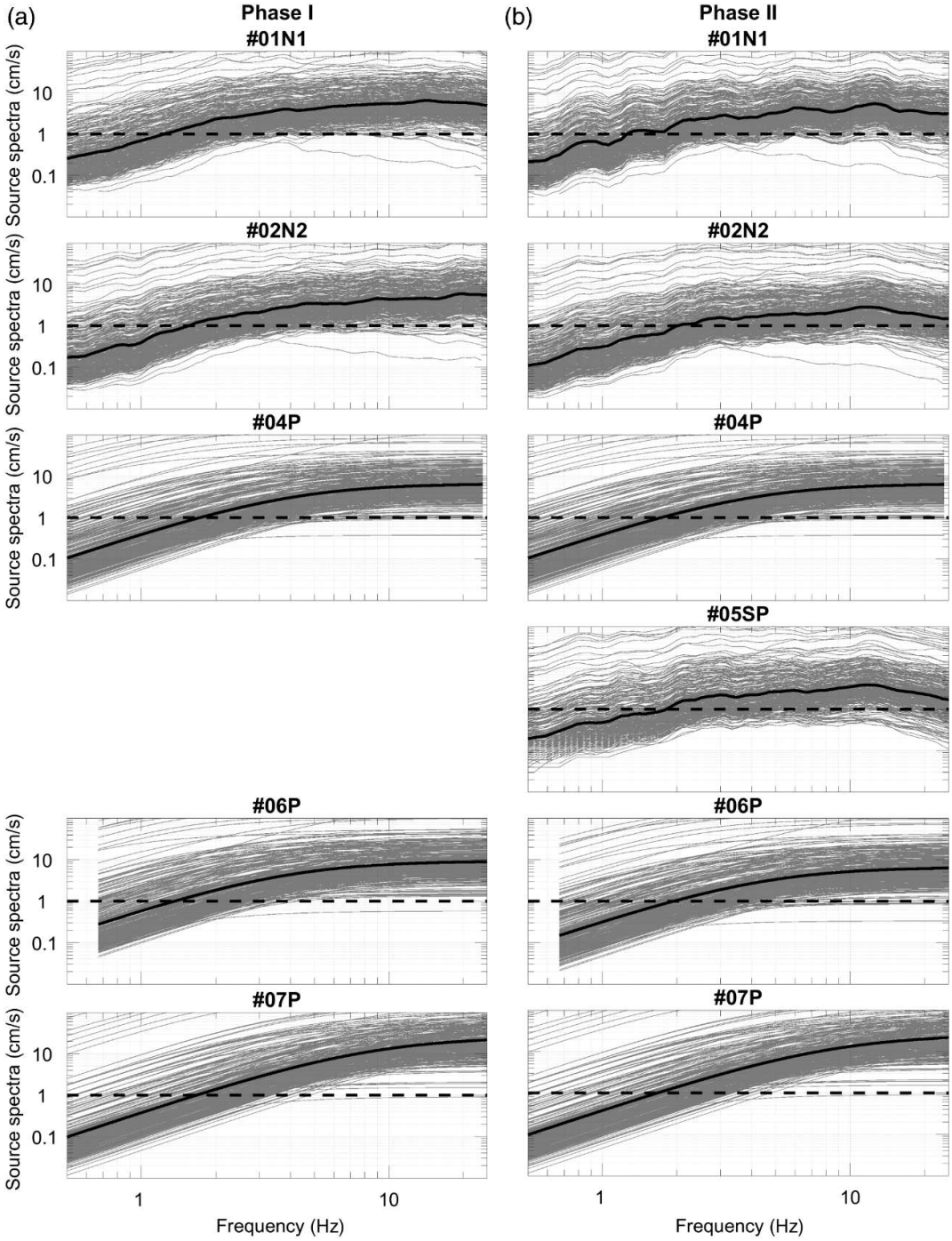

Figure 9. *Italian dataset results for (a) phases I and (b) II. Overall comparisons of the source spectra obtained from the different inversions (as indicated) and showing the means for all of the spectra (bold black).*

logarithmic scale, std($\log_{10}$), for the nonparametric spectra, termed spectral variability. Then, the parametric variability is presented by the coefficient of variation (COV) on the estimated parameters. The use of the COV ensures a variability estimation that does not depend on the mean values. As an alternative, (max−min)/2 is introduced instead of standard deviations and the ratio of (max−min)/(max+min) for COV, in which max and min are the maximum and minimum estimations of the variable considered. This is indicated as the maxmin (MM) estimation in both the cases.

Quantification of the uncertainties

Spectral variability (std and MM of $\log_{10}$). For each event, the nonparametric source spectra, attenuation, and site (from the different inversions) are used to estimate both the standard deviations and MM (in $\log_{10}$). Figure 12 shows

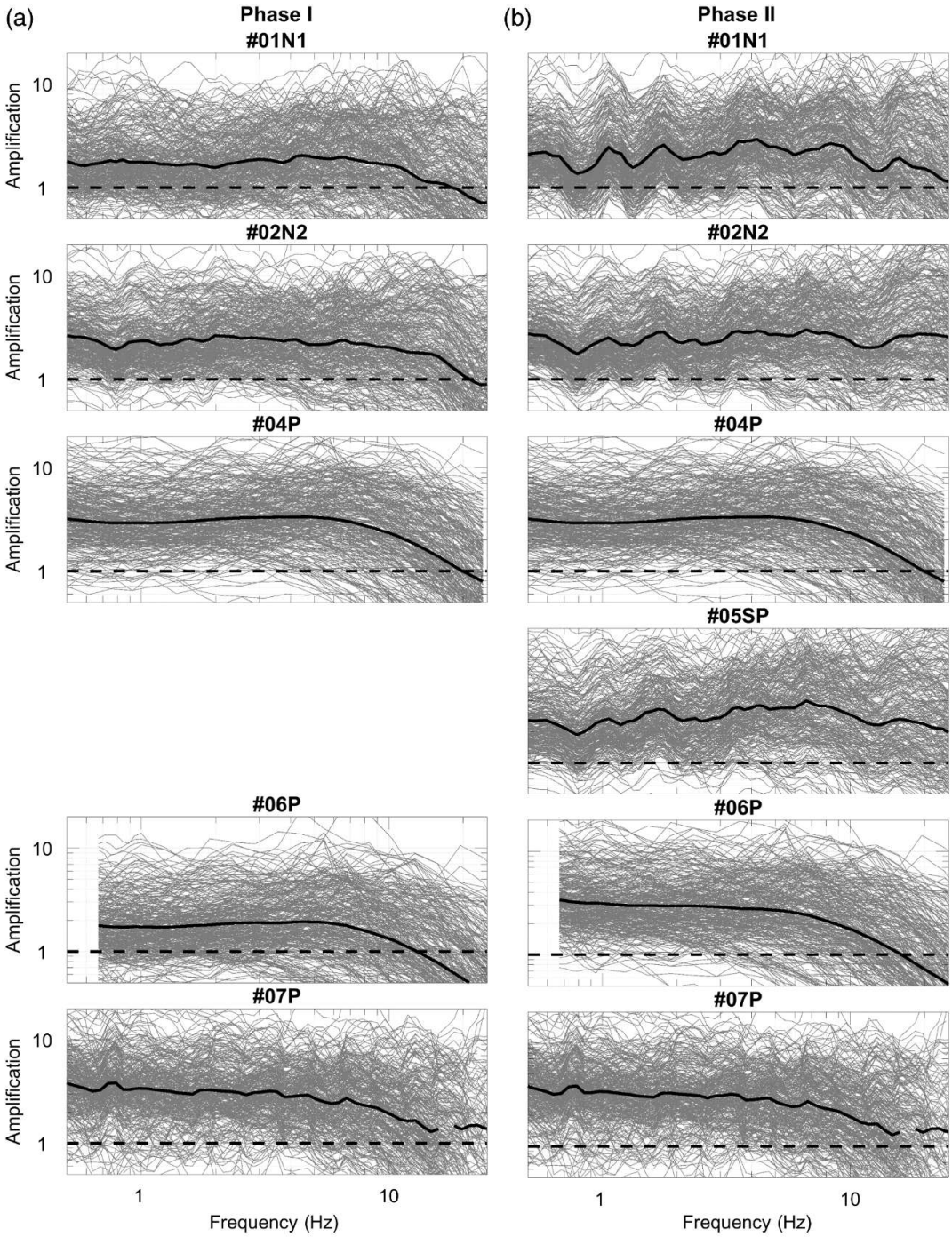

Figure 10. *Central Italian dataset results from phases (a) I and (b) II. Overall comparisons of the site amplifications obtained from the different inversions (as indicated) and showing the means for all of the sites (bold black).*

example site response and source spectra that results from different inversions of phase II of the French and Italian data. The results on each site (and source) are considered to quantify the uncertainty, as described earlier. Similar steps are done for the attenuation curves at each frequency. Then, the estimations are presented for each source and site as functions of the frequency, whereas they are presented as functions of distance and frequency for the attenuation curves, as shown in Figures 13 and 14. The color scale used in Figures 13 and 14 corresponds to the values of the variability estimate (i.e., std($\log_{10}$) or (max−min)/2).

If the panels of Figures 13 and 14 are compared horizontally, it can be seen that the site responses are less prone to variability for both the representations (i.e., std, MM). Also, the synthetic data show an expected minimal variability between the methods, with a tendency for lower

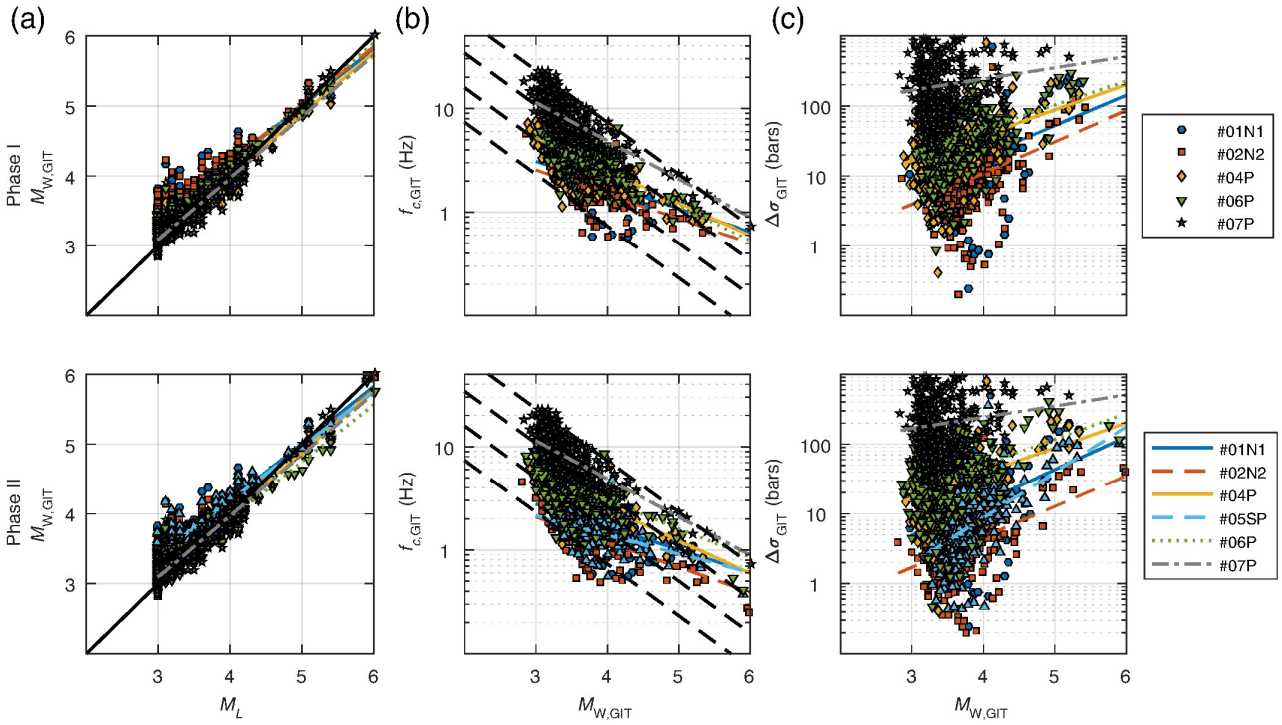

Figure 11. *Central Italian dataset source results. (a) Plot (1:1) of the M_w obtained from the inversions ($M_{w,GIT}$) with respect to the M_L values provided. (b) Distribution of the corner frequencies f_c versus $M_{w,GIT}$ estimated from the inversions. Dashed lines, stress-drop lines of 1, 10, 100, and 1000 bars. (c) Stress-drop distributions from the GIT approaches versus the $M_{w,GIT}$.*

variability for the site terms. The source spectra of the synthetic data show minimal variability of 0.2 (std) and 0.3 (MM), or a factor of 1.5 and 2, respectively, in the linear scale, whereas the variability of the site responses is around 0.1 (for std and MM) or a factor of 1.2. Despite the differences in the mean site responses, the variability of the site responses for the French and Italian datasets is much more limited than for the source terms. The variability of the site terms starts to increase significantly to 0.4 std beyond 10 Hz (factor of 2.5).

If the panels in Figures 13 and 14 are compared vertically, the same term variability for the different datasets can be considered. For example, the sources for the French dataset show high variability that starts at 0.3 std (factor of 3) at low frequencies and exceeds 1 std at high frequencies (factor 10). The Italian dataset shows more consistency in terms of lower variability for the source spectra, which does not exceed 0.2 std (factor 1.5) before 8 Hz and reaches 0.5 std afterward (factor of 3). The attenuation terms show similar variabilities that increase beyond 100 km in both of the real datasets to reach 0.4 std (factor of 3). As for the site responses, similar robustness is achieved up to 10 Hz for both the datasets.

The reduced variability of results from central Italy is probably due to the good geometry and density of the network, which allowed the recording of each event tens or even hundreds of

TABLE 5
Summary of the Mean Estimations of the Attenuation Parameters for Italian Dataset from the Different Inversions for Phases I and II

	Q_0		$Q_{50\,km}$(4 Hz)		α		γ	
Inversion	**Phase I**	**Phase II**	**Phase I**	**Phase II**	**Phase I**	**Phase II**	**Phase I**	**Phase II**
#01N1	5,13,84	358,04	35,81	35,81	0,22	0,40	2,16	2,23
#02N1	150,86	90,95	40,18	49,10	0,64	0,70	1,88	1,37
#03N2	56,13	56,13	51,50	51,50	0,59	0,59	1,26	1,26
#04P	-	45,60	-	82,23	-	0,74	-	1,01
#06P	88,78	98,98	98,87	90,38	0,49	0,46	0,97	1,03
#07P	122,87	122,87	60,07	60,07	0,54	0,54	1,61	1,61

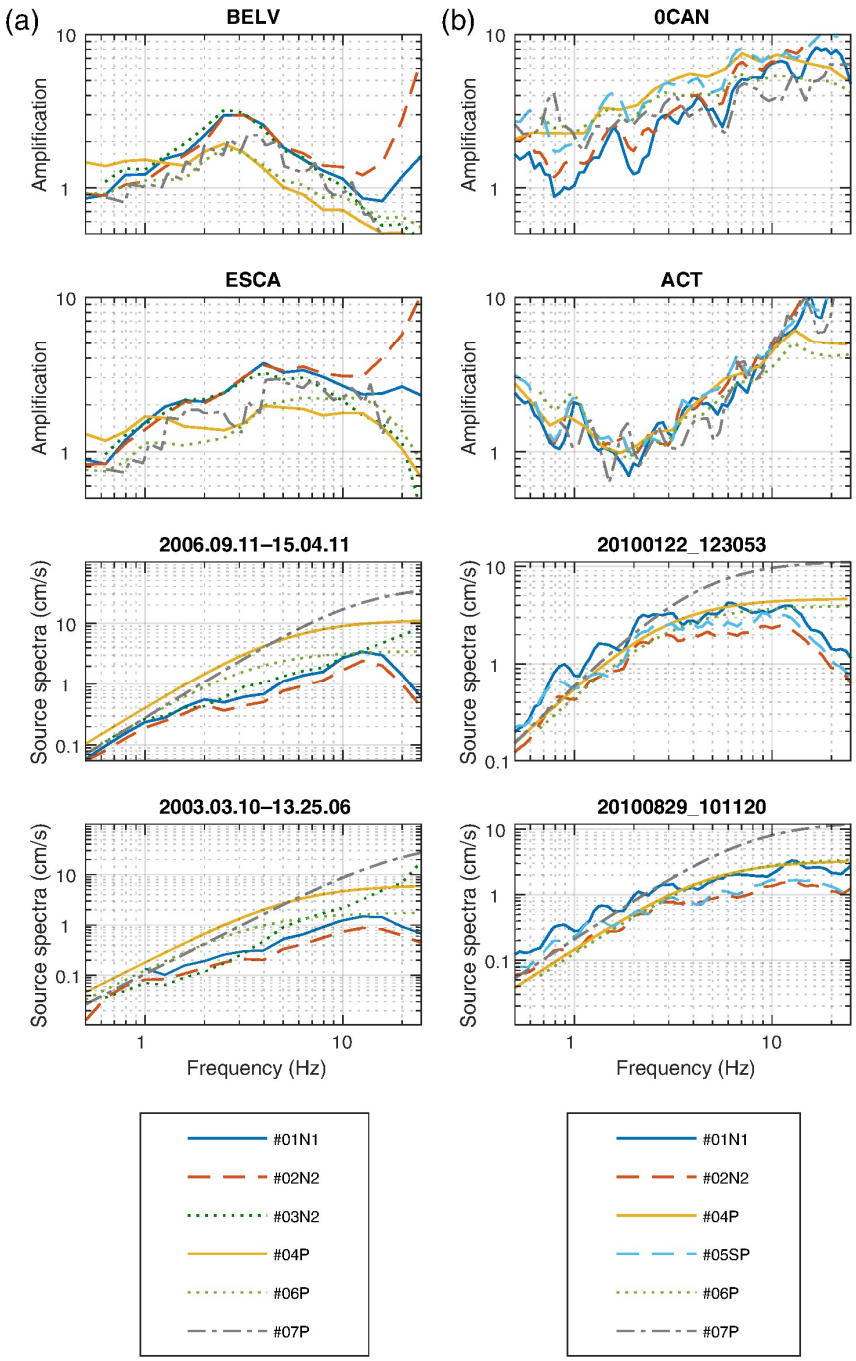

Figure 12. *Example site-response and source spectra results are shown of each of the (a) French and (b) Italian datasets. The results are those obtained from the second phase of the inversions. The names of sites and dates of events are indicated at the top of each figure.*

times. After comparisons between the results from the French and Italian datasets, it appears that the redundancy in the datasets (in terms of the number of recordings, the data sampling for the distance, and magnitude ranges) is essential and helpful to reduce the variability associated with generalized inversions. In other words, the more data there are from the region under study, the lower the intermethod variability.

Source parameter variability (COV and MM). Figures 15 and 16 show the estimations of the variability of the source parameters using COV and MM. For each event, the variability from the six inversion types is assessed with COV and MM. In both the cases, the distributions of these estimations are plotted over constant bins. In each bin, the average number of recordings is reported on the right axis (N_{rec}).

The statistics carried out for the French and Italian datasets show very low intermethod variability for the magnitude M_w, as compared to that for the f_c and $\Delta\sigma$ parameters. Indeed, the variability in terms of seismic moment M_0, which is directly used in the inversions, is higher than for that of M_w. This shows that the deduced M_w has lower variability, as it benefits from the relationship given in equation (4). On the other hand, for the comparison of the two datasets, f_c and $\Delta\sigma$ show very small drops in their variability for central Italy (mainly in Fig. 15). The MM representation shown in Figure 16 appears to limit the variability estimations more, in which fewer bins are obtained than for Figure 15.

Any specific event in the French dataset was recorded on average by 10 sites, whereas for the Italian dataset, the events were recorded on average by 40 sites. This might represent evidence that data redundancy (i.e., to have events covered by as many sites as possible) is important intermethod variability of GIT.

Summary and comparisons of estimated variability. For a representative summary of the variability, we computed the generalized values for each

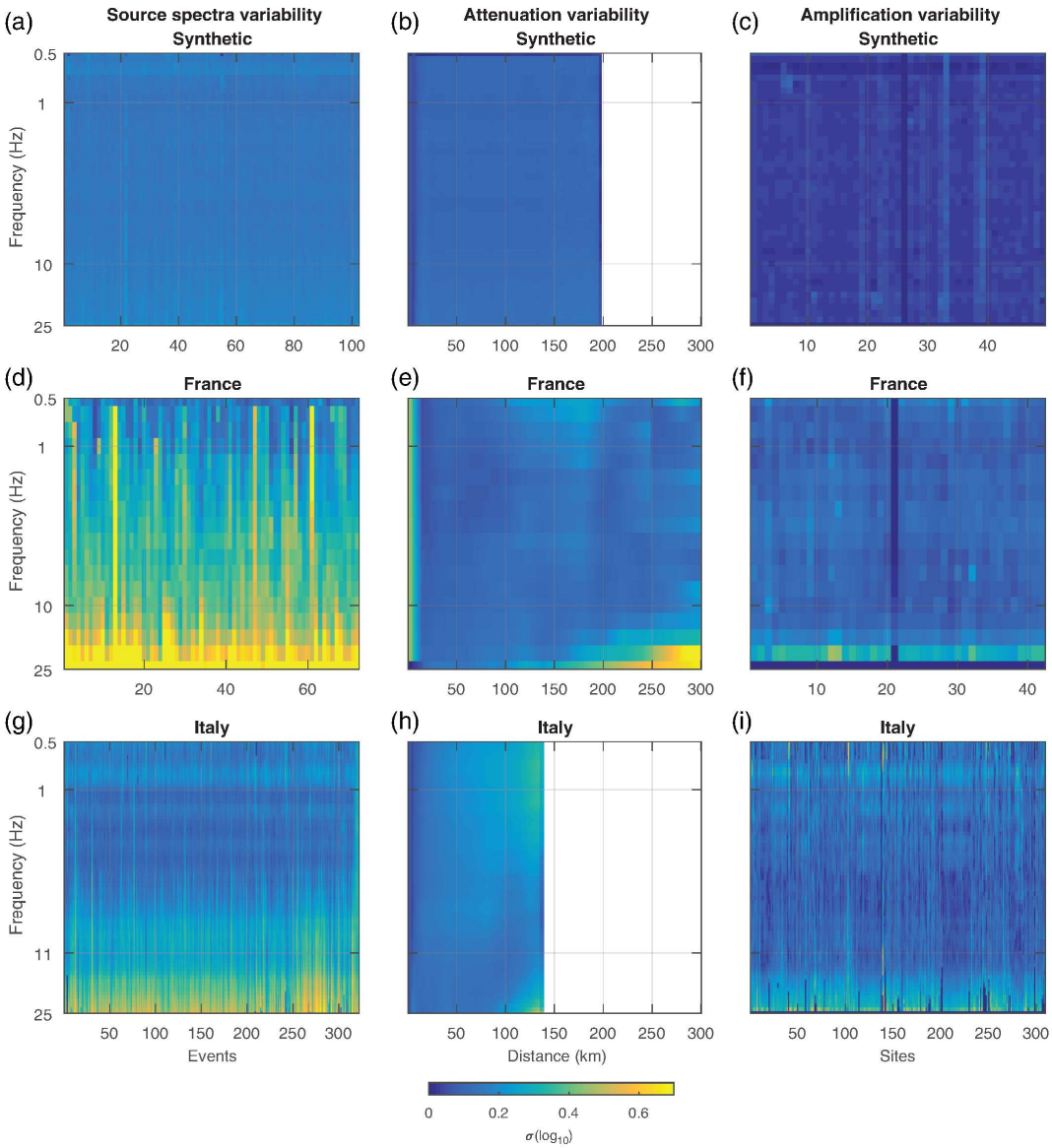

Figure 13. *(a–c) Synthetic, (d–f) France, and (g–i) Italian datasets. Estimations from the constrained phase (i.e., phase II) of the inter-method variabilities (as indicated), as standard deviations of log_{10} at each frequency, for the source spectra and the amplifications obtained after the inversions. The single-color scale is given at the bottom.*

dataset. For the nonparametric curves, the three frequencies of 0.5, 4, and 25 Hz were picked to compute the means of the variability per dataset for all of the sources and sites, and at all distances within the common range for attenuation (i.e., [1–140 km]). Figures 17 and 18 show the values plotted directly instead of in a tabulated form.

Figure 17 shows the mean spectral variability for both the indicators (i.e., std and MM). What can be seen from these comparisons is the high-frequency variability of the sources and sites. However, the highest variability is seen for the source and attenuation terms. The site terms represent the most robust terms of these estimations. Evidently, unifying the reference conditions in phase II did not decrease the variability observed.

The mean COV was also evaluated for all of the events, along with the mean attenuation parameters for each dataset (Fig. 18). Although the MM estimations were generally lower than COV, the two GIT parameters that are most prone to high variability are $\Delta\sigma$ and Q_0. This might serve as a reference for the uncertainty on these parameters using GIT approaches.

Possible origins of variability: regional variations

It is important to start to understand the origins of the variability observed. Therefore, we plotted the regional distributions of the spectral variability of the sources and sites in Figure 13. These

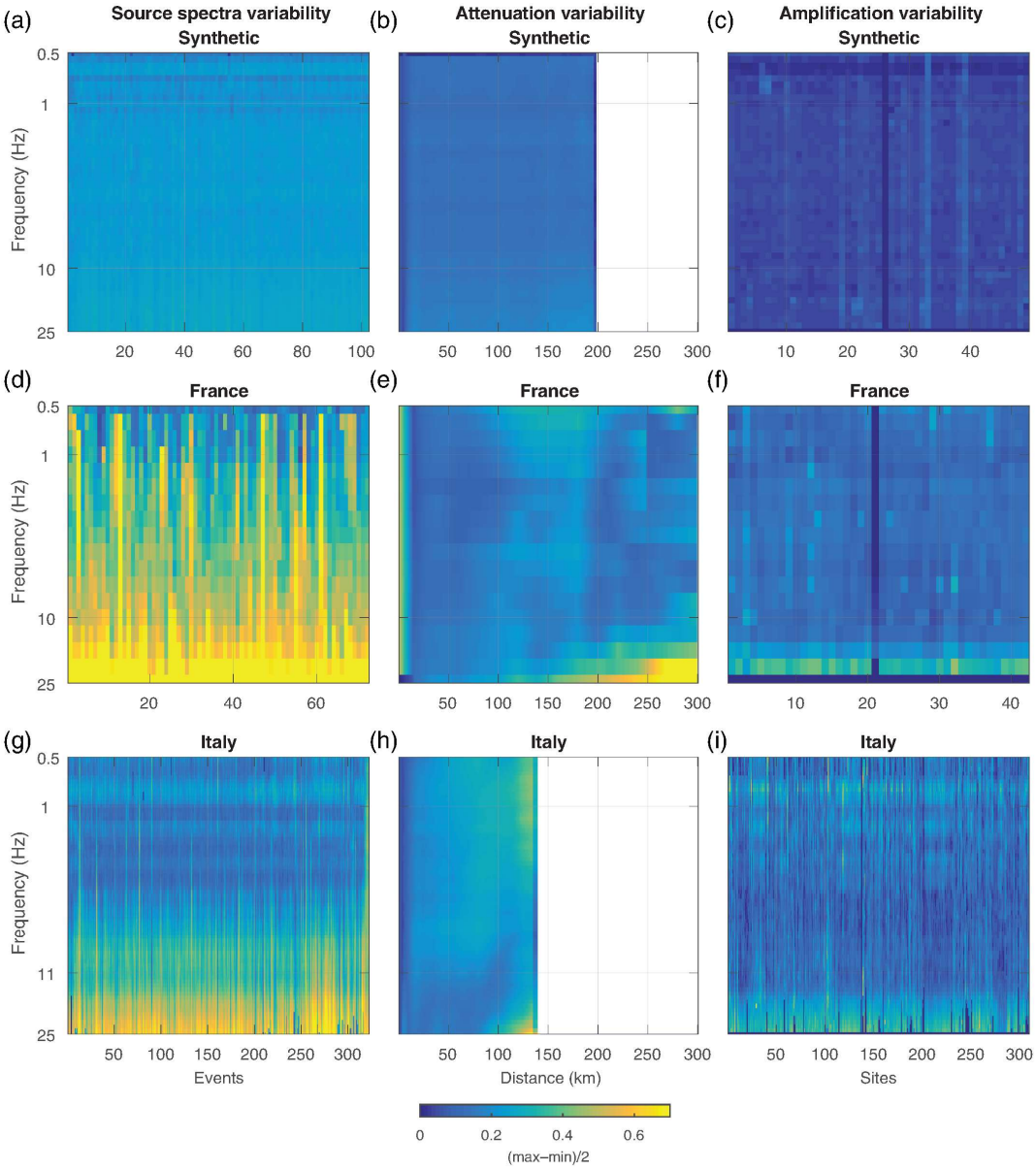

Figure 14. *(a–c) Synthetic, (d–f) France, and (g–i) Italian datasets. Estimations from the constrained phase (i.e., phase II) of the inter-method variabilities (as indicated), as maxmin (MM) of log_{10} at each frequency, for the source spectra and the amplifications obtained after the inversions. The single-color scale is given at the bottom.*

spectra variability values were retrieved from the estimates that are presented in Figures 19 and 20. At each source (or station), the color scale of the marker corresponds to the level of variability (std(log_{10})), whereas the size represents the number of recordings (nb_{rec}). In this way, any regional changes in the variability can be captured.

For the French Alps (Fig. 19), the source spectra variability showed limited regional dependence, whereas the site variability showed regional changes, in particular, at high frequencies. At 4 and 25 Hz, the sites in the southeast of France showed higher variability, although this is not clear at the lower frequency of 0.5 Hz. Going from the north to the south of the Alps, there was increasing variability.

Also, for central Italy (Fig. 20), there were regional changes in the spectral variability, again at high frequencies, in particular. The center of the dataset region (i.e., near the reference station marked in red) contrasts with the northern parts at all frequencies. For example, at high frequency, increasing variability is observed from the center to the northern regions.

We looked for recent studies of regional variations to identify any correlations within the regions considered. Indeed, regional variations are usually addressed in terms of crustal attenuation, in which regionalized maps of attenuation

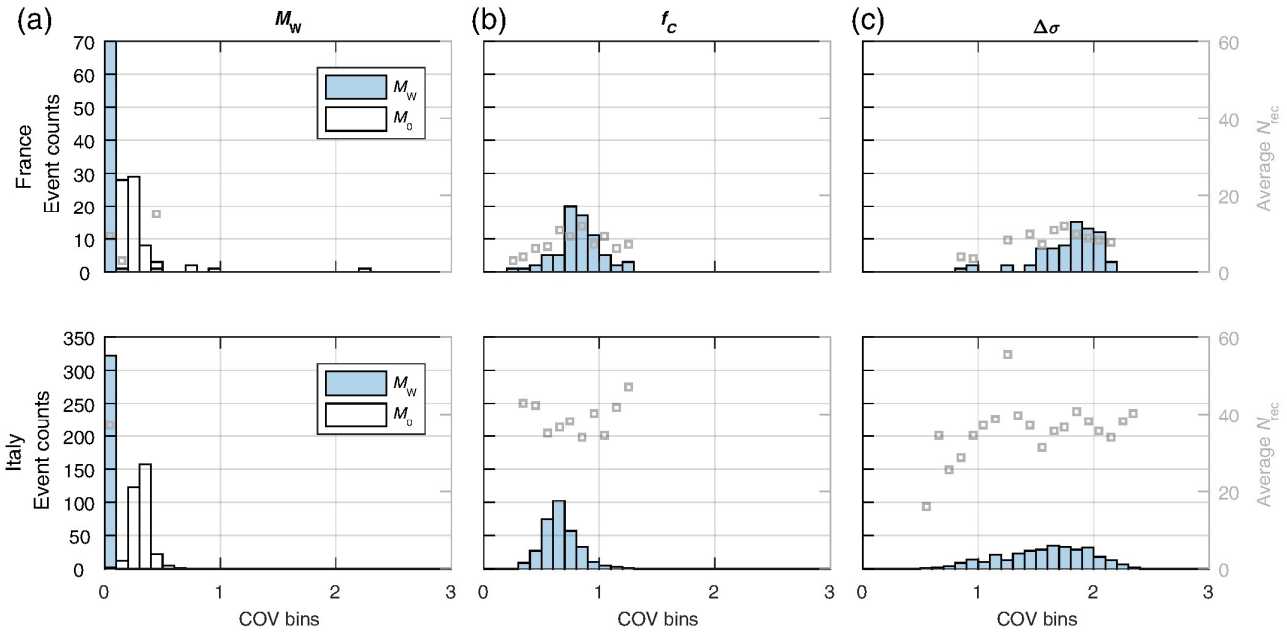

Figure 15. *French and Italian datasets. Estimated variability for each of the source physical parameters (a) M_w, (b) f_c, and (c) $\Delta\sigma$. Variability estimations are grouped into different bins of constant coefficient of variation (COV) width (0.1). For each bin, the mean numbers of recording sites (N_{rec}) is also shown.*

characteristics are established using attenuation tomography studies, such as those of Mayor et al. (2016, 2018), in the European context. Indeed, these previous studies mainly used the coda waves to estimate quality factors from tens of thousands of recordings, and they displayed the results on maps that showed the lateral variations of the frequency-dependent quality factors.

After detailed comparisons of these maps, several aspects can be mentioned. First, within the French dataset, the variability changes at high frequencies tended to match the attenuation variations in the maps of Mayor et al. (2016), who focused on regions that included the southeast of France. Although the source variability was not clear, the site variability changed from higher values at higher attenuation in the south of the dataset region to lower values with lower attenuation in the north. On the other hand, the Italian dataset shows that there was low variability with fewer attenuation zones in the center than the northern parts at high frequencies. As a result, most of the higher variability (either for source or site) is seen in the higher attenuation zones.

In summary, in high attenuation regions, we observed more variability compared to those of low attenuation. A direct interpretation of these correlations might be that regional variations of attenuation that were not accounted for in the GIT inversions and models led to increased variability. The tradeoffs allow this variability to be transmitted to either the source or the site or both the terms.

EXPLORING THE IMPACT OF THE DATASET SIZE

After the illustration of these results, we were interested in investigating the impact of a lack of redundant data on the inversion results. For this, a "decimated" subset of the French dataset was used as follows:

- the number of sites was reduced from 42 to 14;
- the number of events was reduced from 72 to 24;
- the recordings per station and event (with conserving a lower bound, >3) were reduced from 645 to 107; and
- the dataset referred to the OGCH hard-rock site as the chosen reference site.

With all of the other features remaining the same as for the initial GITEC French dataset, the inversion schemes of teams #01N1 (nonparametric) and #04P (parametric) were applied to both the original and this decimated dataset.

Examples of the results for two events are illustrated in Figure 21. These two inverted source spectra show that larger changes affected the nonparametric GIT spectra when the data were reduced than the parametric GIT spectra. The

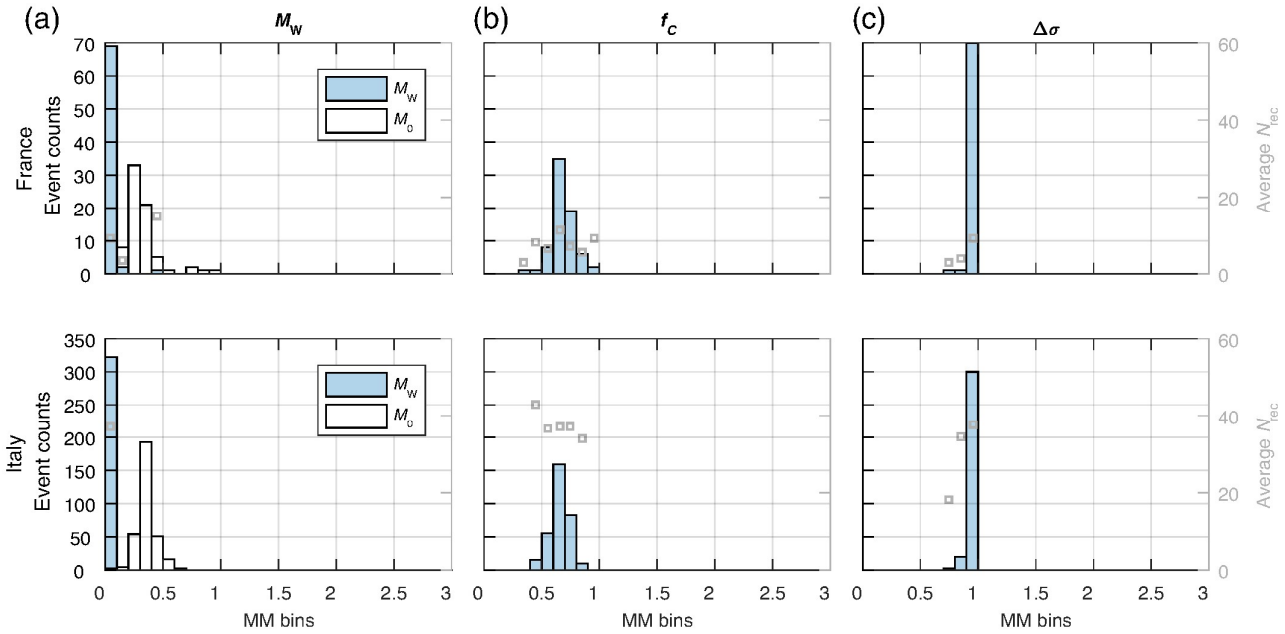

Figure 16. *French and Italian datasets. Estimated MM for each of the source physical parameters (a) M_w, (b) f_c, and (c) $\Delta\sigma$. MM estimations are grouped into different bins of constant MM width (0.1). For each bin, the mean numbers of recording sites (N_{rec}) is also shown.*

ratios between the new and initial inverted spectra provide a clear illustration of the factors of the changes that occurred. In a second step, the mean ratio was computed (over all of the frequencies), and the events were grouped into bins following their mean ratio.

Applying the same procedure to the inverted site amplifications, Figure 20 also shows the distributions of the mean ratios obtained over the events and sites considered for both of the GIT methods. This ratio for events inverted with #01N1 covers a range of 0–5, whereas that for #04P remains limited. On the contrary, the site responses for the decimated dataset appear to be less affected for both the methods.

These changes in the inverted spectra will definitely affect the physical parameter estimates, especially as it was not possible to postfit some of the source spectra for the nonparametric method to a Brune model. This indicates the failure of the inversion to retrieve the event spectra when there are very few records available. Following these observations, it appears that the nonparametric GIT approach results in less reliable source spectra when there are reduced amounts of data compared with the parametric GIT approaches. Here, we deduce the nonreliability in this test by the significant impact on results before and after the data decimation. These observations seem reasonable, because in the parametric approach the source spectrum has fixed a priori form, unlike the case in the nonparametric approach.

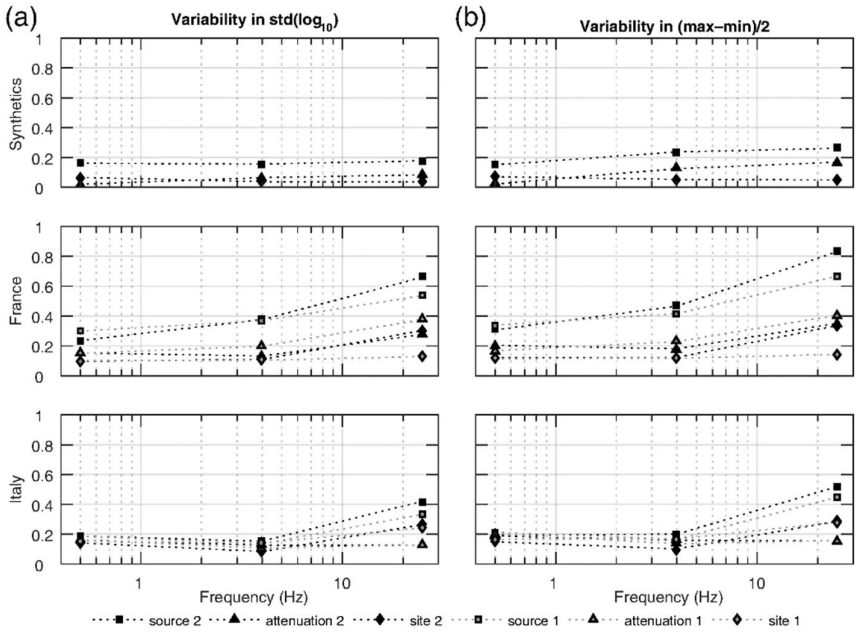

Figure 17. *Phase I and II mean spectral variability estimations in terms of (a) standard deviations of log_{10} and (b) MM of log_{10}. These estimations are shown by considering all the events, the attenuation at distances between [0–140 km], and all the sites. Three frequency points are considered.*

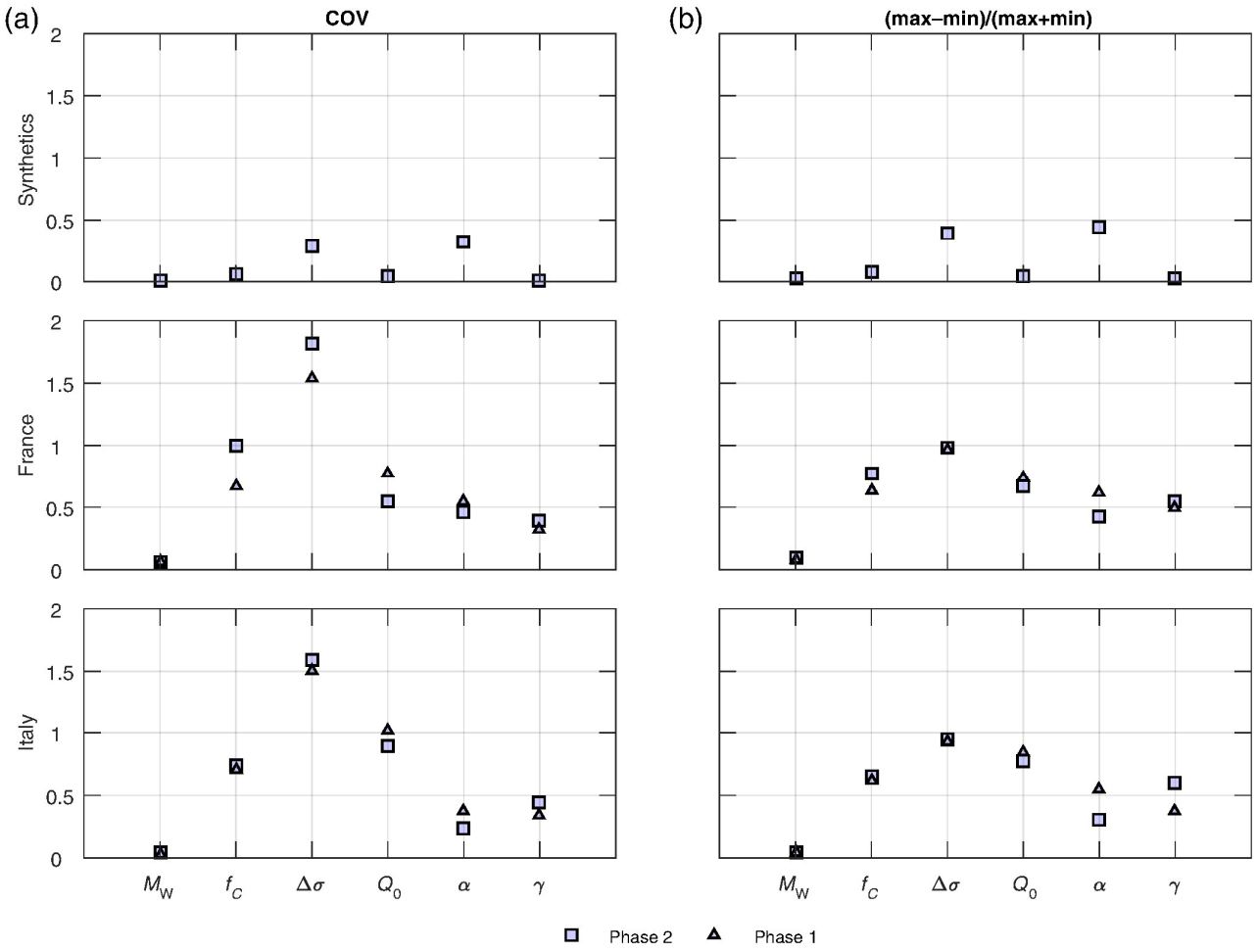

Figure 18. *Phases I and II mean parameter variabilities, in terms of (a) COV and (b) MM of log_{10}, for all the event and attenuation parameters delivered by the different GIT approaches.*

SUMMARY AND CONCLUSIONS

The main observations and conclusions can be summarized as:

- The attenuation characteristics of the regions considered appear to be more complicated than the simple homogenous quality factor. Significant attenuation changes with distance and regional variations of attenuations are behind the variability observed for the attenuation curves obtained. Also, such simple Q models can result in very unstable estimations of the attenuation parameters.
- The site terms appear to show the lowest variability (on average, a factor of 1.2 below 10 Hz and 1.5 beyond 10 Hz) among the different results, in which site references can have important roles in terms of the average site responses in the dataset considered.
- The source terms appear to be subject to high variability with a factor 3 at low frequency that increases to factor of 5 at high frequency, in the French dataset. Data redundancy is important to decrease this variability over all the frequencies, as in the Italian dataset (i.e., sufficient numbers of recordings per event and site).
- The M_w source parameter shows less variability among the different approaches (factor 0.1 around the mean value) than the corner frequency (f_c) and the stress drops ($\Delta\sigma$), with factors reaching 0.7 and 1.7 around the mean value, respectively. This might be a result of the way that the parameterization uses M_0 directly, instead of M_w. The relation used to deduce M_w from M_0 ($M_w \propto \log_{10}(M_0)$) leads to reduced variability in the results for M_w.
- The comparisons after data decimation suggest that the nonparametric scheme tends to deliver less reliable source terms when the amount of data is reduced, whereas the site response remains more stable. Thus, keeping the dataset updated with recordings and including new stations can provide essential benefits for nonparametric GIT approaches.

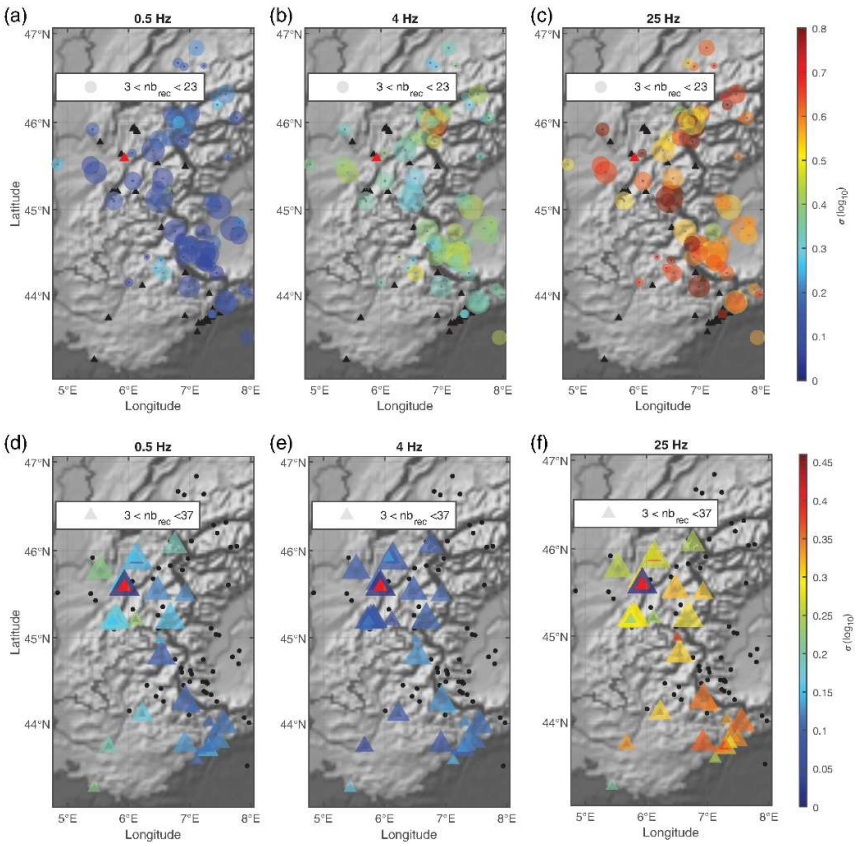

Figure 19. *French dataset. Maps of the variabilities for the (a–c) sources and (d–f) sites in terms of std of log_{10} at three different frequency points (0.5, 4, and 25 Hz). Triangles and circles, stations, and earthquakes, respectively; symbol size, proportional to number of recordings; symbol color, intermethod variability at the given site or source.*

Based on the different approaches used (i.e., parametric, nonparametric), each appears to have its own pros and cons relative to the desired application. With relatively few data in a given dataset, applying a nonparametric approach appears to be counter-indicated for both source and attenuation. For example, the attenuation model derived for such an approach can only be defined using the source–site distance points in the dataset. In contrast, with a parametric approach, the model assumed from the beginning is calibrated through the inversion iterations to fit the recorded data characteristics.

Nonparametric GIT is accompanied by an indirect assumption made on the source by defining the attenuation curves to start from unity at the reference distance "R_{ref}." This assumption implies that all sources are shifted to the R_{ref}, whereby the attenuation starts from unity at this distance. This can be a very approximate assumption when there are little or no data in the short-distance range (e.g., <50 km).

On the other hand, nonparametric approaches appear to provide more information about earthquake sources and regional attenuation than parametric approaches, because the unmodeled source spectra and attenuation curves can be visualized with fewer a priori assumptions. Therefore, an important aspect is to reduce the a priori assumptions as much as possible to improve the adequacy of the models.

For the preference between the GIT methods, several points can be mentioned. Where there is a sufficient amount of data, the nonparametric approach represents a reliable tool. Because nonparametric inversions estimate source and attenuation models based on the data, then the richer the data, the more robust the models are inverted. On the other hand, GIT on small datasets would be better carried out according to parametric inversion schemes under the conditions that provide the necessary constraints for the inversions from a priori knowledge.

Following the several aspects indicated earlier related to the reliability of GIT at high frequencies, several questions can be posed. First, it can be directly proposed that reducing the assumptions on sources (i.e., nonparametric spectra, instead of the Brune model) might be the reason behind the high-frequency discrepancies. In other words, the source spectra can follow a multiple corner frequency form. For example, the study of Bindi et al. (2019) that used data from central Italy proposed a source model that was anchored by a parameter they called "κ_{source}". This confirmation for the presence of high-frequency slope for sources can only be accepted if the inversion schemes are shown to be stable and free of high-frequency trade-offs. Thus, the high-frequency performance of the inversion schemes remains under question. On the other hand, if the susceptibility of the nonparametric inversions to trade-offs is accepted, then these

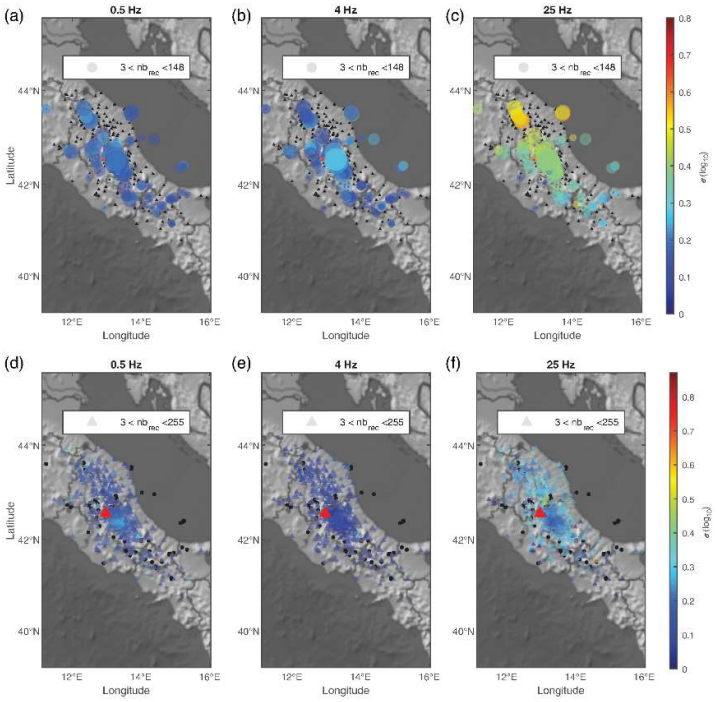

Figure 20. *Italian dataset. Maps of the variabilities for the (a–c) sources and (d–f) sites in terms of std of log_{10} at three different frequency points (0.5, 4, and 25 Hz). Triangles and circles, stations, and earthquakes, respectively; symbol size, proportional to number of recordings; symbol color, inter-method variability at the given site or source.*

of corresponding results.

Several additional questions need to be explorated in the future to improve the understanding of the variability and its origins. For instance, synthetic datasets can be used to address specific questions such as the accounting of regional variations and depth dependence of attenuation. Also, additional aspects of dataset configurations are interesting to explore (e.g., the impact of the seismological network geometry with respect to earthquake location and vice versa). This might help to improve the efficiency of future inversions by providing optimized datasets. In addition, the minimum and maximum magnitude limits below (or above), which the corner frequencies can be resolved by the inversions appears to be an interesting question. Finally, it seems interesting to address the possibility of capturing more complicated seismic-wave phenomena using GIT approaches, such as differences at high frequency can be misleading. Thus, the parametric models (especially the Brune model) might be preferred instead of accepting that these trade-offs occur. However, the final answer to this question about the high-frequency performance of GIT methods remains relatively unclear, and needs further investigations and testing.

To conclude, the preference of either a parametric or a nonparametric approach does not appear straightforward, in general. The preference might be case dependent, based on the dataset of interest (e.g., the amount of data available). However, as the best practice, we propose that it is best to proceed carefully with both the approaches in parallel, with continuous comparisons of the results from the different approaches before their direct application and the use

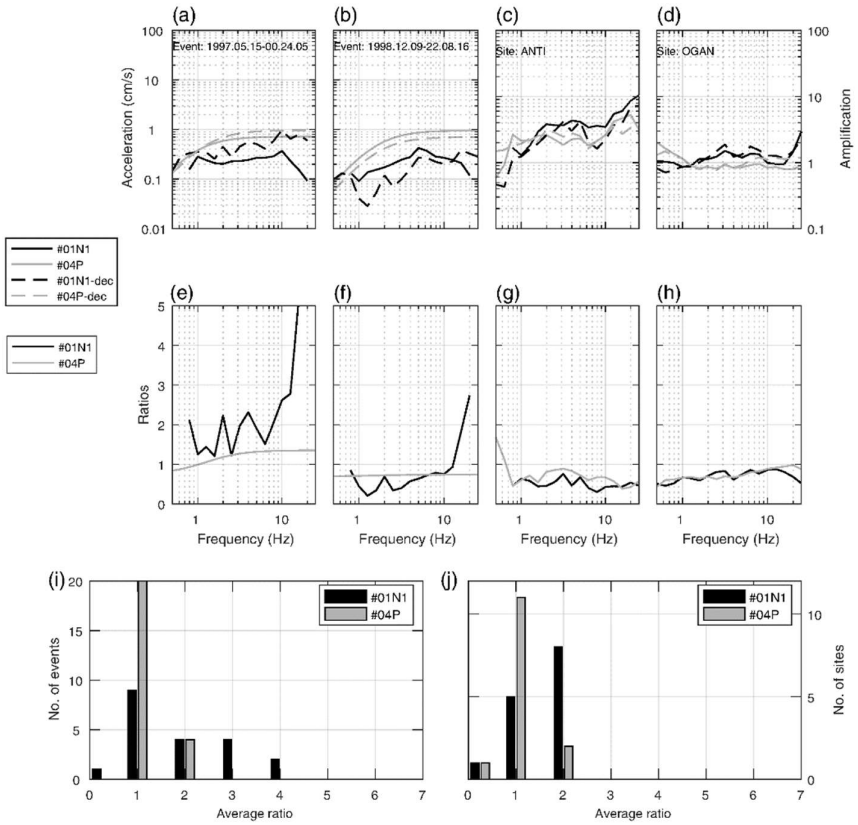

Figure 21. *Decimated French dataset. (Top) Examples of the sources for the two (a,b) events and (c,d) sites as considered in two inversions: once with the whole French dataset (solid lines) and once with the decimated dataset (dashed lines). (e–h) Ratios of the curves in panels (a)–(d) (i.e., between the whole and decimated datasets). (Bottom) Distributions of the mean ratios defined for all of the events (i) and the sites (j), as obtained after each of the inversions performed.*

extending the assumptions on the point-source models generally used in GIT and for stochastic ground-motion simulations.

DATA AND RESOURCES

The datasets used in this work came from published papers listed in the references. They were obtained after the direct request of authors of these listed papers.

DECLARATION OF COMPETING INTERESTS

The authors acknowledge that there are no conflicts of interest recorded.

ACKNOWLEDGMENTS

Thanks for Francesca Pacor (National Institute of Geophysics and Volcanology [INGV] Milano), Daniele Spallarossa (University of Genova), and Stephane Drouet (Fugro, France) for providing the French and central Italian data used in this text. Thanks for the two reviewers and for Thomas Pratt for their valuable comments that helped improve the text.

REFERENCES

Andrews, D. J. (1986). Objective determination of source parameters and similarity of earthquakes of different size, in Earthquake Source Mechanics, S. Das, J. Boatwright, and C. H. Scholz (Editors), Geophysical Monograph Series, Vol. 37, American Geophysical Union, Washington, D.C., 259–267, doi: 10.1029/GM037p0259.

Bard, P.-Y., and J.-C. Gariel (1986). The seismic response of two-dimensional sedimentary deposits with large vertical velocity gradients, Bull. Seismol. Soc. Am. 76, no. 2, 343–366.

Bard, P.-Y., S. S. Bora, F. Hollender, A. Laurendeau, and P. Traversa (2020). Are the standard VS-kappa host-to-target adjustments the only way to get consistent hard-rock ground motion prediction? Pure Appl. Geophys. 177, no. 5, 2049–2068, doi: 10.1007/s00024-019-02173-9.

Bindi, D., F. Pacor, L. Luzi, M. Massa, and G. Ameri (2009). The Mw 6.3, 2009 L'Aquila earthquake: Source, path and site effects from spectral analysis of strong motion data, Geophys. J. Int. 179, no. 3, 1573–1579, doi: 10.1111/j.1365-246X.2009.04392.x.

Bindi, D., S. Parolai, H. Grosser, C. Milkereit, and S. Karakisa (2006). Crustal attenuation characteristics in northwestern Turkey in the range from 1 to 10 Hz, Bull. Seismol. Soc. Am. 96, no. 1, 200–214, doi: 10.1785/0120050038.

Bindi, D., M. Picozzi, D. Spallarossa, F. Cotton, and S. R. Kotha (2019). Impact of magnitude selection on aleatory variability associated with ground-motion prediction equations: Part II—Analysis of the between-event distribution in central Italy, Bull. Seismol. Soc. Am. 109, no. 1, 251–262, doi: 10.1785/0120180239.

Bindi, D., D. Spallarossa, and F. Pacor (2017). Between-event and between-station variability observed in the Fourier and response spectra domains: Comparison with seismological models, Geophys. J. Int. 210, no. 2, 1092–1104, doi: 10.1093/gji/ggx217.

Boore, D. M. (2003). Simulation of ground motion using the stochastic method, Pure Appl. Geophys. 160, no. 3, 635–676, doi: 10.1007/PL00012553.

Bora, S. S., F. Scherbaum, N. Kuehn, P. Stafford, and B. Edwards (2015). Development of a response spectral ground-motion prediction equation (GMPE) for seismic-hazard analysis from empirical fourier spectral and duration models, Bull. Seismol. Soc. Am. 105, no. 4, 2192–2218, doi: 10.1785/0120140297.

Brune, J. N. (1970). Tectonic stress and the spectra of seismic shear waves from earthquakes, J. Geophys. Res. 75, no. 26, 4997–5009, doi: 10.1029/JB075i026p04997.

Brune, J. N. (1971). Seismic sources, fault plane studies and tectonics, Eos Trans. AGU 52, no. 5, IUGG 178–IUGG 187, doi: 10.1029/EO052i005pIU178.

Cadet, H., P.-Y. Bard, and A. Rodriguez-Marek (2012). Site effect assessment using KiK-net data: Part 1. A simple correction procedure for surface/downhole spectral ratios, Bull. Earthq. Eng. 10, no. 2, 421–448, doi: 10.1007/s10518-011-9283-1.

Castro, R. R., J. G. Anderson, and S. K. Singh (1990). Site response, attenuation and source spectra of S waves along the Guerrero, Mexico, subduction zone, Bull. Seismol. Soc. Am. 80, no. 6A, 1481–1503.

Drouet, S., S. Chevrot, F. Cotton, and A. Souriau (2008). Simultaneous inversion of source spectra, attenuation parameters, and site responses: Application to the data of the French accelerometric network, Bull. Seismol. Soc. Am. 98, no. 1, 198–219, doi: 10.1785/0120060215.

Drouet, S., F. Cotton, and P. Guéguen (2010). v S30, κ, regional attenuation and Mw from accelerograms: Application to magnitude 3–5 French earthquakes, Geophys. J. Int. 182, no. 2, 880–898, doi: 10.1111/j.1365-246X.2010.04626.x.

Drouet, S., and F. Cotton (2015). Regional stochastic GMPEs in low? seismicity areas: Scaling and aleatory variability analysis—Application to the French Alps, Bull. Seismol. Soc. Am. 105, no. 4, 1883–1902, doi: 10.1785/0120140240.

Edwards, B., and D. Fäh (2017). Prediction of earthquake ground motion at rock sites in Japan: Evaluation of empirical and stochastic approaches for the PEGASOS Refinement Project, Geophys. J. Int. 211, no. 2, 766–783, doi: 10.1093/gji/ggx328.

Edwards, B., A. Rietbrock, J. J. Bommer, and B. Baptie (2008). The acquisition of source, path, and site effects from microearthquake recordings using Q tomography: Application to the United Kingdom, Bull. Seismol. Soc. Am. 98, no. 4, 1915–1935, doi: 10.1785/0120070127.

Eshelby, J. D. (1957). The determination of the elastic field of an ellipsoidal inclusion, and related problems, Proc. Royal Soc. Lond. 241, no. 1226, 376–396, doi: 10.1098/rspa.1957.0133.

Goertz-Allmann, B. P., and B. Edwards (2014). Constraints on crustal attenuation and three-dimensional spatial distribution of stress drop in Switzerland, Geophys. J. Int. 196, no. 1, 493–509, doi: 10.1093/gji/ggt384.

Grendas, I., N. Theodoulidis, F. Hollender, and P. Hatzidimitriou (2021). A GIT algorithm for simultaneous estimation of seismic source, site response and regional-distance dependent attenuation parameters: Application to synthetic and real data, J. Seismol. 25, no. 2, 575–598, doi: 10.1007/s10950-020-09975-8.

Hanks, T. C., and H. Kanamori (1979). A moment magnitude scale, J. Geophys. Res 84, no. B5, 2348–2350, doi: 10.1029/JB084iB05p02348.

Hollender, F., C. Cornou, A. Dechamp, K. Oghalaei, F. Renalier, E. Maufroy, C. Burnouf, S. Thomassin, M. Wathelet, P.-Y. Bard, et al. (2018). Characterization of site conditions (soil class, VS30, velocity profiles) for 33 stations from the French permanent accelerometric network (RAP) using surface-wave methods, Bull. Earthq. Eng. 16, no. 6, 2337–2365, doi: 10.1007/s10518-017-0135-5.

Kawase, H., F. Nagashima, K. Nakano, and Y. Mori (2019). Direct evaluation of S-wave amplification factors from microtremor H/V ratios: Double empirical corrections to "Nakamura" method, Soil Dynam. Earthq. Eng. 126, 105067, doi: 10.1016/j.soildyn.2018.01.049.

Kennett, B. L. N. (1974). Reflections, rays, and reverberations, Bull. Seismol. Soc. Am. 64, no. 6, 1685–1696.

Klin, P., G. Laurenzano, C. Barnaba, E. Priolo, and S. Parolai (2021). Site amplification at permanent stations in northeastern Italy, Bull. Seismol. Soc. Am. 111, no. 4, 1885–1904, doi: 10.1785/0120200361.

Klin, P., G. Laurenzano, and E. Priolo (2018). GITANES: A MATLAB package for estimation of site spectral amplification with the generalized inversion technique, Seismol. Res. Lett. 89, no. 1, 182–190, doi: 10.1785/0220170080.

Kotha, S. R., D. Bindi, and F. Cotton (2016). Partially nonergodic region specific GMPE for Europe and Middle-East, Bull. Earthq. Eng. 14, no. 4, 1245–1263, doi: 10.1007/s10518-016-9875-x.

Laurendeau, A., P.-Y. Bard, F. Hollender, V. Perron, L. Foundotos, O.-J. Ktenidou, and B. Hernandez (2018). Derivation of consistent hard rock (1000 < VS < 3000 m/s) GMPEs from surface and down-hole recordings: Analysis of KiK-net data, Bull. Earthq. Eng. 16, no. 6, 2253–2284, doi: 10.1007/s10518-017-0142-6.

Lee, V. W., and M. D. Trifunac (2010). Should average shear-wave velocity in the top 30m of soil be used to describe seismic amplification? Soil Dynam. Earthq. Eng. 30, no. 11, 1250–1258, doi: 10.1016/j.soildyn.2010.05.007.

Mayor, J., M. Calvet, L. Margerin, O. Vanderhaeghe, and P. Traversa (2016). Crustal structure of the Alps as seen by attenuation tomography, Earth Planet. Sci. Lett. 439, 71–80, doi: 10.1016/j.epsl.2016.01.025.

Mayor, J., P. Traversa, M. Calvet, and L. Margerin (2018). Tomography of crustal seismic attenuation in metropolitan France: Implications for seismicity analysis, Bull. Earthq. Eng. 16, no. 6, 2195–2210, doi: 10.1007/s10518-017-0124-8.

Nakano, K., S. Matsushima, and H. Kawase (2015). Statistical properties of strong ground motions from the generalized spectral inversion of data observed by K-NET, KiK-net, and the JMA Shindokei Network in Japan, Bull. Seismol. Soc. Am. 105, no. 5, 2662–2680, doi: 10.1785/0120140349.

Oth, A., D. Bindi, S. Parolai, and D. D. Giacomo (2011). Spectral analysis of K-NET and KiK-net data in Japan, Part II: On attenuation characteristics, source spectra, and site response of borehole and surface stations, Bull. Seismol. Soc. Am. 101, no. 2, 667–687, doi: 10.1785/0120100135.

Oth, A., H. Miyake, and D. Bindi (2017). On the relation of earthquake stress drop and ground motion variability, J. Geophys. Res. 122, no. 7, 5474–5492, doi: 10.1002/2017JB014026.

Pacor, F., D. Spallarossa, A. Oth, L. Luzi, R. Puglia, L. Cantore, A. Mercuri, M. D'Amico, and D. Bindi (2016). Spectral models for ground motion prediction in the L'Aquila region (central Italy): Evidence for stress-drop dependence on magnitude and depth, Geophys. J. Int. 204, no. 2, 697–718, doi: 10.1093/gji/ggv448.

Parolai, S., D. Bindi, M. Baumbach, H. Grosser, C. Milkereit, S. Karakisa, and S. Zünbül (2004). Comparison of different site response estimation techniques using aftershocks of the 1999 Izmit earthquake, Bull. Seismol. Soc. Am. 94, no. 3, 1096–1108, doi: 10.1785/0120030086.

Perron, V., P.-Y. Bard, F. Hollender, C. Gélis, C. Guyonnet-Benaize, B. Hernandez, and O.-J. Ktenidou (2017). Robustness of kappa (κ) measurement in low-to-moderate seismicity areas: Insight from a site-specific study in provence, France, Bull. Seismol. Soc. Am. 107, no. 5, 2272–2292, doi: 10.1785/0120160374.

Rodriguez-Marek, A., F. Cotton, N. A. Abrahamson, S. Akkar, L. A. Atik, B. Edwards, G. A. Montalva, and H. M. Dawood (2013). A model for single-station standard deviation using data from various tectonic regions, Bull. Seismol. Soc. Am. 103, no. 6, 3149–3163, doi: 10.1785/0120130030.

Traversa, P., E. Maufroy, F. Hollender, V. Perron, V. Bremaud, H. Shible, S. Drouet, P. Guéguen, M. Langlais, D. Wolyniec, et al. (2020). RESIF RAP and RLBP dataset of earthquake ground motion in mainland France, Seismol. Res. Lett. 91, no. 4, 2409–2424, doi: 10.1785/0220190367.